Structure–function correlations in oxygen activating non-heme iron enzymes

Michael L. Neidig and Edward I. Solomon*

Received (in Cambridge, UK) 18th July 2005, Accepted 20th October 2005
First published as an Advance Article on the web 16th November 2005
DOI: 10.1039/b510233m

A large group of mononuclear non-heme iron enzymes exist which activate dioxygen to catalyze key biochemical transformations, including many of medical, pharmaceutical and environmental significance. These enzymes utilize high-spin Fe^{II} active sites and additional reducing equivalents from cofactors or substrates to react with O_2 to yield iron-oxygen intermediates competent to transform substrate to product. While Fe^{II} sites have been difficult to study due to the lack of dominant spectroscopic features, a spectroscopic methodology has been developed which allows the elucidation of the geometric and electronic structures of these active sites and provides molecular level insight into the mechanisms of catalysis. This review provides a summary of this methodology with emphasis on its application to the determination of important active site structure–function correlations in mononuclear non-heme iron enzymes. These studies provide key insight into the mechanisms of oxygen activation, active site features that contribute to differences in reactivity and, combined with theoretical calculations and model studies, the nature of oxygen intermediates active in catalysis.

I. Introduction

An extensive group of mononuclear and binuclear non-heme iron metalloenzymes exist which activate dioxygen for key biochemical reactions in organisms ranging from bacteria to humans.[1] The mononuclear non-heme iron enzymes comprise a large and expanding collection of oxygen activating enzymes catalyzing reactions of medical, pharmaceutical and environmental significance as wide and diverse as those of heme enzymes. However, the chemistry of the mononuclear non-heme iron enzymes can be very different from their heme counterparts due to electronic and geometric differences arising from their ligand environments. The heme porphyrin ligand allows for delocalization of the iron d-orbitals into the heme π cloud and the iron sites in heme enzymes are often low spin as compared to non-heme enzymes which are generally high-spin. In addition, the presence of a planar, tetradentate heme ligand imposes steric constraints on the iron site that are not present in the non-heme enzymes. Despite these important geometric and electronic differences, the mononuclear non-heme iron enzymes had generally been less well studied due to their lack of the characteristic intense porphyrin $\pi \rightarrow \pi^*$ transitions present in heme enzymes and the fact that it is the

Department of Chemistry, Stanford University, Stanford, CA 94305, USA. E-mail: edward.solomon@stanford.edu

Michael L. Neidig received his BA (summa cum laude) in chemistry from Colgate University and a Churchill Fellowship to Churchill College, University of Cambridge where he was awarded an MPhil in chemistry. He received a National Science Foundation graduate fellowship to pursue PhD studies in chemistry at Stanford University under the direction of Professor Edward I. Solomon. His research interests include structure–function correlations in the mononuclear non-heme iron enzymes, focusing on the lipoxygenases and the α-KG and related dioxygenases.

Edward I. Solomon grew up in North Miami Beach, FL, received his PhD from Princeton University (with D. S. McClure) and was a postdoctoral fellow at the H. C. Orsted Institute (with C. J. Ballhausen) and then at CalTech (with H. B. Gray). He was a professor at MIT until 1982. He then moved to Stanford University where he is the Monroe E. Spaght Professor of Humanities and Sciences. He is a member of the National Academy of Sciences, the American Academy of Arts and Sciences and a Fellow of the American Association for the Advancement of Science. His awards include the ACS Award in Inorganic Chemistry, the Remsen Award from the Maryland ACS, the Centenary Medal of the Royal Society of Chemistry, the Wheland Medal from the University of Chicago, the Frontiers in Biological Chemistry Award from the Max Planck Institute in Mülheim, the ACS Award for Distinguished Service in the Advancement of Inorganic Chemistry and the Deans Award for Distinguished Teaching at Stanford. He has presented a large number of named lectures including the first Glen Seaborg Lecture at the University of California-Berkeley and has been an Invited Professor at a number of international universities. His research is in the fields of physical-inorganic and bioinorganic chemistry with emphasis on the application of a wide variety of spectroscopic and computational methods to elucidate the electronic structures of transition metal complexes and their contributions to physical properties and reactivity. Areas of present interest are structure–function correlations in mono- and binuclear non-heme iron enzymes, O_2 and N_2O activation and reduction by mono-, bi-, tri- and tetranuclear copper active sites and electronic structure contributions to electron transfer in copper, iron-sulfur and heme sites.

Fe^{II} sites that are often reactive and yet these lack intense absorption features and have integer spin $S = 2$ ground states which are generally EPR silent. Our understanding of the active site structures and mechanisms of dioxygen activation in the mononuclear non-heme iron enzymes has greatly expanded in recent years due to more extensive biochemical and kinetic analyses, the application of spectroscopic methods capable of probing the electronic transitions of high-spin Fe^{II} sites and the availability of an increasing number of high resolution crystal structures.

At present, the mononuclear non-heme iron enzymes involved in dioxygen activation can be divided into two general groups as shown in Table 1: (A) substrate activating and (B) dioxygen activating enzymes. Substrate activating enzymes are characterized by their utilization of high-spin Fe^{III} sites to activate organic substrates for direct reaction with dioxygen and include the lipoxygenases and the intradiol dioxygenases. Lipoxygenases catalyze the regio- and stereospecific hydroperoxidation of 1,4-*Z*,*Z*-pentadiene-containing polyunsaturated carboxylic acids in plants and animals.[2–5] In humans, lipoxygenases produce leukotrienes and lipoxins, signaling molecules that mediate important biological processes such as asthma, atherosclerosis and cancer.[6–9] Current insight into the molecular mechanism of lipoxygenase derives from a variety of kinetic and spectroscopic studies of soybean lipoxygenase (sLO) due to its ease of purification and stability. Crystallographic studies of Fe^{II} sLO have shown the iron active site to be either four- or six-coordinate, both having one terminal carboxylate ligand from Ile839 and three histidine ligands (His690, His504 and His499), where the coordination differences observed arise from the definition of whether the Asn694 carbonyl O is a ligand and whether there is a water ligand also present.[10–12] Circular dichroism (CD) and magnetic circular dichroism (MCD) studies of resting sLO helped resolve this discrepancy having shown the active site to be a 40/60 mixture of five-coordinate (5C) and six-coordinate (6C) Fe^{II} species which becomes purely 6C upon substrate binding.[13] The enzyme must be oxidized to the Fe^{III} state for activity. The generally accepted mechanism for sLO involves H-atom abstraction from the C11 position of the substrate by an Fe^{III}–OH,[14] shown to be a 5C species by EPR,[15] resulting in an Fe^{II}–OH_2 species and a substrate radical.[14,16–18] This coordination flexibility (6C Fe^{II} → 5C Fe^{III}), attributed to the Asn694 ligand, has been proposed to play an important role in tuning the active site for catalysis. Density Functional Theory (DFT) calculations on H-atom abstraction by the Fe^{III}–OH^- site of sLO have shown that the coordination flexibility contributes to the reaction energetics by stabilizing

Table 1 Classification of mononuclear non-heme iron enzymes

A. Substrate activating	
Lipoxygenases	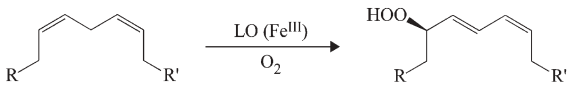
Intradiol dioxygenases	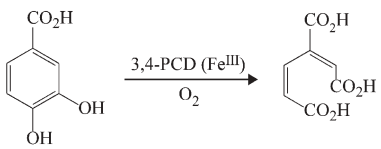
B. Oxygen activating	
Extradiol dioxygenases	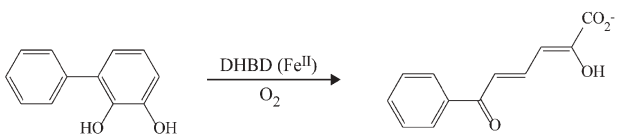
Pterin-dependent hydroxylases	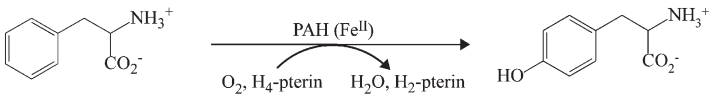
α-KG-dependent dioxygenases	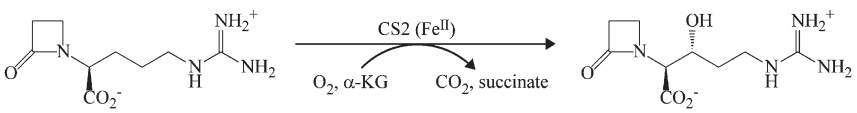
Rieske dioxygenases	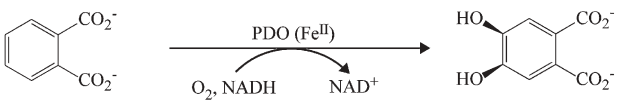
Bleomycin	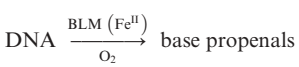

the Fe^{II} relative to the Fe^{III} state, raising the redox potential and the pK_a of the water ligand of the reduced site.[19] The transition state for H-atom abstraction is best described as a proton coupled electron transfer (PCET) process as the electron tunnels directly from the substrate to the iron through a superexchange pathway involving an Fe–O-**H**-substrate bridge (where **H** is the hydrogen being transferred). Dioxygen would react directly with the substrate radical formed in the PCET process to yield a peroxyl radical which subsequently oxidizes the Fe^{II}–OH_2 to give the active Fe^{III}–OH^- site and the hydroperoxidated product, 13-HPOD ([(9*Z*,11*E*)-13-hydroperoxy-9,11-octadecadienoic acid]).

The intradiol dioxygenases, involved in the aerobic degradation of nearly all naturally occurring and xenobiotic aromatic compounds, catalyze the ring cleavage of *cis*-hydroxylated aromatic compounds between the hydroxylated carbons. Extensive studies of one member of this class, protocatechuate 3,4-dioxygenase (3,4-PCD), have provided a detailed understanding of the active site structure and mechanism of the intradiol dioxygenases. Numerous crystal structures of 3,4-PCDs exist including those of the resting, substrate bound and substrate analog bound Fe^{III} complexes.[20–25] The resting structure shows a distorted trigonal bipyramidal Fe^{III} center with histidine (His462) and tyrosinate (Tyr447) as the axial ligands and histidine (His460), tyrosinate (Tyr408) and typically a water-based ligand in the equatorial plane. X-ray absorption spectroscopy (XAS) has supported the nature of the water-based ligand being hydroxide. The characteristic burgundy red color of all the intradiol dioxygenases is due to the tyrosine ligation and the resulting tyrosinate ligand-to-metal charge transfer transitions (LMCT).[26–29] Kinetic, spectroscopic and crystallographic studies have shown the displacement of the axial tyrosinate and equatorial hydroxide ligands by substrate, which binds bidentately to Fe^{III} in a doubly deprotonated form.[20–23,30–32] The substrate complex changes geometry to square pyramidal with an open coordination position *trans* to His460 and has asymmetric substrate chelation, with a longer Fe^{III}–$O_{substrate}$ bond *trans* to Tyr408. While substrate binding to the Fe^{III} center of 3,4-PCD leads to activation of the substrate for direct reaction with dioxygen, the mechanism of intradiol activation and cleavage remains unclear. Proposed mechanisms for substrate activation and intradiol reactivity involve elongation of this Fe^{III}–$O_{substrate}$ bond to facilitate ketonization of the substrate C3–O during oxygen attack[33] and covalent binding of the catecholate as a donor ligand to induce radical character in the ring.[34,35] Binding of the distal oxygen of the resulting peroxy-substrate intermediate to the vacant coordination position *trans* to His460 would subsequently promote both O–O bond cleavage and intradiol ring cleavage.

Oxygen activating mononuclear non-heme iron enzymes utilize an Fe^{II} resting site which directly binds O_2 to yield iron-oxygen intermediates which react with substrate to yield product. These enzymes can be classified (Table 1B) based upon the source of the extra reducing equivalents required for oxygen activation since the one electron reduction of dioxygen is unfavorable due to its low redox potential and the resulting weak Fe^{III}–O_2^- bond that would form.[36] The extradiol dioxygenases are a class of oxygen activating mononuclear non-heme iron enzymes that utilize substrates (cathecholates) which themselves carry all the reducing equivalents necessary for oxygen activation and, therefore, do not require a cosubstrate (*i.e.* intramolecular dioxygenases).[1,33] While the intra- and extradiol dioxygenases both catalyze ring cleavage of *cis*-diol-containing aromatic compounds, the extradiol dioxygenases utilize a high-spin Fe^{II} resting site to cleave catechols specifically on either the proximal or distal side of the hydroxyl groups. Direct insight into the Fe^{II} active site structure of the extradiols derived from crystallographic and CD/MCD studies of the resting and substrate-bound forms of catechol 2,3-dioxygenase and 2,3-dihydroxybiphenyl 1,2-dioxygenase (DHBD), which showed the presence of 5C square pyramidal sites in both the resting and substrate-bound enzymes.[37–41] Additional insight into the nature of the catecholate–Fe^{II} interaction derives from the crystallography and UV resonance Raman[42] of the DHBD–substrate complex which showed that the substrate, 2,3-dihydroxybiphenyl, binds bidentately to Fe^{II} as the monoanion in an asymmetric fashion ($Fe–O_{substrate}$ = 2.0 and 2.4 Å) by displacing two water ligands. EXAFS and MCD studies of this species have also shown the presence of a strong, axial Fe^{II}–glutamate bond in the substrate-bound complex.[40] The 5C DHBD/Fe^{II}/substrate complex reacts with dioxygen to yield product by a mechanism yet unknown.

The crystallographic data on the extradiol dioxygenases show that the ligation sphere of the resting Fe^{II} site consists of two histidine and one carboxylate amino acid derived ligands arranged on one face of an octahedron. This structural motif at the Fe^{II} active site, termed the 2-His-1-carboxylate facial triad, is common to most of the Fe^{II} mononuclear non-heme iron enzymes which activate dioxygen.[43–45] In the resting sites of these enzymes, the remaining coordination positions of Fe^{II} are occupied by water (*e.g.* three water ligands in phenylalanine hydroxylase (PAH) and the α-KG dioxygenases) or contain two water ligands and one vacant site (*e.g.* extradiol dioxygenases).[1] Interestingly, for the Rieske dioxygenases and pterin-dependent hydroxylases where neither substrate nor cofactor bind directly to Fe^{II}, the carboxylate ligand of the facial triad has been found to act as a bidentate ligand though any possible role of this ligation in catalysis remains unclear.[45] It should also be noted that for human homogentisate dioxygenase, the resting crystal structure also shows possible bidentate coordination of the carboxylate ligand though the substrate, homogentisate, likely coordinates directly to Fe^{II}.[46] Thus, the Fe^{II} sites of mononuclear non-heme enzymes have three non-amino acid ligated coordination positions accessible to bind substrates, cofactors and/or dioxygen. This contrasts with the heme enzymes which have the four equatorial positions occupied by the heme ligand with one axial position occupied by an amino acid derived ligand (commonly histidine or cysteine), leaving only one exchangeable position which is the site of oxygen binding. Alternatively, the substrate activating enzymes lipoxygenase and the intradiol dioxygenases utilize a more extensive set of amino acid ligands than simply the facial triad, likely due to the different requirements of their mechanisms of catalysis (*i.e.* tuning redox potentials in the LOs and using strong tyrosine ligands to stabilize Fe^{III} sites to activate substrate for direct reaction

with dioxygen in the intradiol dioxygenases). While the facial triad is commonly observed, several mononuclear non-heme Fe^{II} enzymes which activate dioxygen exist which have somewhat different ligation spheres. One such example is isopenicillin N synthase (IPNS), which has an additional amino acid derived ligand, glutamine, *trans* to one of the histidines of the facial triad.[47] However, substrate binding in IPNS leads to displacement of the glutamine ligand by direct coordination of the substrate to Fe^{II}.[48]

The pterin-dependent hydroxylases require Fe^{II}, tetrahydrobiopterin (BH_4) and O_2 to catalyze the aromatic hydroxylation of important amino acid residues and include the phenylalanine, tyrosine and tryptophan hydroxylases.[49] In this class of enzymes it is the BH_4 cosubstrate which supplies two additional electrons for oxygen activation. Phenylalanine hydroxylase, which catalyzes the conversion of L–Phe to L–Tyr, has been extensively studied due to the fact that dysfunction of this enzyme has been associated with the genetic disorder phenylketonuria.[50,51] While many studies of Fe^{III} PAH have been reported due to its spectroscopic accessibility, CD, MCD and XAS studies of the catalytically active Fe^{II} form of the enzyme have provided detailed insight into its geometric and electronic structure.[52–54] Resting Fe^{II} PAH is a distorted 6C site which is not significantly affected by binding of either substrate L–Phe or the cofactor analogue 5-deaza-6-methyltetrahydropterin, neither of which directly coordinates to Fe^{II}. Importantly, the simultaneous binding of both substrate and cofactor results in a 5C Fe^{II} site with an open coordination position available for dioxygen activation, where extended X-ray absorption fine structure (EXAFS) analysis supports the loss of water ligation in the 6C $\rightarrow$ 5C conversion.[54] These structural studies are consistent with kinetic studies showing an ordered mechanism in PAH in which the quaternary complex with Fe^{II}, BH_4 and L–Phe bound must be formed before any product is released.[55–57] While no intermediate in the reaction of pterin-dependent hydroxylases has been observed, a C4a-hydroperoxy-BH_2 has been frequently proposed as one intermediate along the reaction pathway resulting from initial reaction of O_2 with the BH_4 cosubstrate.[58] Subsequent generation of a high valent Fe^{IV}=O intermediate in the proposed mechanism would yield aromatic hydroxylation *via* electrophilic attack of the aromatic ring, consistent with the NIH shift experimentally observed for the reaction.[59]

The α-ketoglutarate (α-KG)-dependent dioxygenases comprise a large and expanding class of mononuclear non-heme iron enzymes which require Fe^{II}, α-KG and dioxygen for catalysis, with the α-KG cosubstrate supplying the two additional electrons required for dioxygen activation.[60] In organisms ranging from humans to bacteria, members of this class play key roles in a broad range of primary and secondary metabolic pathways, perfoming a diverse array of chemical transformations during biosynthesis. These include hydroxylation (prolyl-4-hydroxylase,[61] taurine dioxygenase (TauD)[62]), desaturation and oxidative ring closure (clavaminate synthase, CS2[63–65]) and oxidative ring expansion (deacetoxycephalosporin C synthase, DAOCS[66]). Many members of this class are of particular medical importance as they have been shown to repair N-methylation lesions in DNA,[67–69] be involved in oxygen sensing and response to hypoxia in cells,[70] contribute to the biosynthesis of cephalosporin antibiotics[66] and cross-link collagen.[61] In these systems, the resting, substrate, and α-KG bound forms are all six coordinate (6C), with α-KG bound to Fe^{II} in a bidentate fashion as shown by CD/MCD spectroscopy[71–73] and crystallographic studies.[74–77] The binding of cofactor contrasts the other cofactor dependent enzymes and reflects the fact that α-KG must be activated for reaction with dioxygen. Simultaneous binding of both α-KG and substrate leads to conversion to a five coordinate (5C) site, which reacts with O_2 leading to decarboxylation of the α-keto acid to generate CO_2, succinate and oxygen intermediates. Recently, the first direct characterization of an iron-oxygen intermediate trapped in the reaction pathway of an α-KG-dependent dioxygenase has been achieved in TauD, where Mössbauer (δ = 0.31 mm s^{-1}, ΔE_Q = 0.88 mm s^{-1}),[78] resonance Raman ($\upsilon_{Fe=O}$ = 821 cm^{-1})[79] and EXAFS ($r_{Fe=O}$ = 1.62 Å)[80] studies support its identification as an Fe^{IV}=O species. This species reacts with substrate by H-atom abstraction in TauD, followed by rebound hydroxylation by the resulting Fe^{III}–OH^- species, to yield hydroxylated product. In CS2, the Fe^{IV}=O intermediate is capable of catalyzing three reactions: hydroxylation, oxidative ring closure and desaturation.

A sub-class of α-KG-dependent enzymes exist which are unique in that they incorportate both atoms of dioxygen into a single substrate as the α-keto acid moiety is covalently attached to the substrate. These parallel the extradiol dioxygenases, where the catecholate substrate also supplies the extra electrons required for O_2 activation. One member of this sub-class is (4-hydroxyphenyl)pyruvate dioxygenase (HPPD), which catalyzes the conversion of (4-hydroxyphenyl)-pyruvate (HPP) to homogentisate as part of tyrosine catabolism.[81] Another member is 4-hydroxymandelate synthase (HmaS), which uses the same substrate (HPP) as HPPD but forms a different product, (*S*)-4-hydroxymandelate, a secondary metabolite incorporated into antibiotics including vancomycin and complestatin.[82] Interestingly, these enzymes exhibit different iron-oxygen intermediate reactivities, electrophilic attack (HPPD) and H-atom abstraction (HmaS). Several enzymes also exist which are not α-KG dependent but show high sequence homology to the α-KG-dependent dioxygenases. These include IPNS (previously mentioned) which catalyzes the synthesis of isopenicillin *N*, an important precursor molecule in the biosynthesis of all penicillin and cephalosporin antibiotics,[83] and 1-aminocyclopropyl-1-carboxylate oxidase (ACCO) which catalyzes the biosynthesis of the gaseous plant hormone ethylene (*i.e.* the ethylene forming enzyme, EFE).[84,85]

The Rieske dioxygenases are characterized by their use of Fe^{II}, O_2 and bound Rieske [2Fe–2S] clusters, one electron donors ($Fe^{III}Fe^{II} \rightarrow Fe^{III}Fe^{III}$) with two Cys on one iron and two His on this second redox active iron, to catalyze the *cis*-dihydroxylation of unactivated aromatic substrates and play an important biological role in the environmentally significant biodegradation of aromatic compounds from both natural and industrial sources.[86] CD and MCD studies of the non-heme Fe^{II} active site of phthalate dioxygenase (PDO), one member of this class which catalyzes the *cis*-dihydroxylation of

phthalate to 1,2-dihydroxy-4,5-dicarboxy-3,5-cyclohexadiene, provided initial insight into the structure of the resting and substrate-bound forms of Rieske dioxygenases.[87,88] While resting PDO has a 6C Fe^{II} site, binding of phthlate led to the conversion of this site to a mixture of 5C species, creating a coordinatively unsaturated Fe^{II} site for O_2 binding and activation in the presence of substrate. Subsequent crystallographic studies of naphthalene 1,2-dioxygenase (NDO), a Rieske dioxygenase which catalyzes the *cis*-hydroxylation of naphthalene to form (+)-*cis*-(1*R*,2*S*)-dihydroxy-1,2-dihydronapthalene, have provided additional insight into the active site structures of this class of enzymes.[89] It was found that the α3β3 oxygenase component of NDO contains both the mononuclear iron and Rieske centers in the α subunits separated by 44 Å. The observation that the quaternary structure of the oxygenase component places each Rieske cluster within 12 Å of the mononuclear iron site on the adjacent α subunit has led to the proposal that electrons are transferred from the Rieske to the mononuclear iron between subunits during catalysis. Since the reactions of reduced Rieske dioxygenases with dioxygen initially involve the transfer of one electron from the Rieske center and one electron from the non-heme Fe^{II} center, the iron-oxygen intermediate expected to be formed is formally a high-spin Fe^{III}-peroxide species.[90–93] Recently, a peroxide bound side on (η^2) to iron has been observed in a crystal structure of NDO with the alternative substrate indole bound,[94] supporting a high-spin Fe^{III}-peroxide as the catalytically relevant iron-oxygen intermediate in this class of enzymes. Note that in the crystal structure of NDO the resting Fe^{II} site appears to be 5C which still has to be correlated to spectroscopy.

Bleomycin (BLM) is a histidine containing glycopeptide antibiotic used to treat head and neck cancer, testicular cancer and Hodgkin's disease due to its ability to achieve both single- and double-strand DNA cleavage at certain 5′-GC-3′ and 5′-GT-3′ sites in the presence of metal ions, in particular Fe^{II}, and O_2.[95–99] While no crystal structure of Fe^{II}BLM has yet been reported, a combination of MCD spectroscopy and EXAFS has shown the Fe^{II} site to be 6C with one weak axial ligand and the presence of back-bonding between Fe^{II} and a pyrimidine ligand in the equatorial plane of the BLM ligand.[100] The other ligands are believed to be the imidiazole, deprotonated amide, and both the primary and secondary amines of the β-aminoalanine fragment, and the carbamoyl substituent on the mannose sugar.[101] Kinetic and spectroscopic studies have shown that this high-spin Fe^{II} complex reacts with dioxygen and an additional electron to generate activated BLM, a low-spin Fe^{III} hydroperoxide complex.[102–106] Activated BLM reacts by H-atom abstraction from the C4′ position of the deoxyribose sugar of DNA leading to DNA degradation with base propenal formation.

From the above survey, application of an Fe^{II} methodology involving a combination of CD, MCD and variable-temperature variable-field (VTVH) MCD has provided detailed insight into the active site geometric and electronic structures of mononuclear non-heme iron enzymes. Following a brief overview of this CD/MCD/VTVH-MCD methodology, this review focuses on its application to determine structure–function correlations over non-heme Fe^{II} enzymes that activate dioxygen. Findings from these studies include: (1) a general structural mechanism for the control oxygen activation in the presence of cosubstrates, (2) active site features that contribute to differences in reactivity (*e.g.* aliphatic and aromatic hydroxylation, desaturation), and (3) the relationship of mutations at the active site to disease states. In addition, the recent availability of structural, spectroscopic and computational data on the resulting iron-oxygen intermediates in enzymes and models provide the basis for an overview of the nature of oxygen intermediates in these enzymes and their reactivity.

II. Methodology

Determination of the splitting of the five d-orbitals of the Fe^{II} active site provides key information on mononuclear non-heme iron enzymes. These splittings depend upon the ligand environment of the Fe^{II} and directly relate to the geometric and electronic structures of the sites and, thus, their reactivities. A high-spin Fe^{II} (d^6) free ion has a ^5D ground state which splits in energy in various ligand environments. In an octahedral ligand field, the ^5D splits into a triply degenerate $^5T_{2g}$ (*i.e.* $S = 2$) ground state and a doubly degenerate ^5E_g excited state at $10Dq(O_h)$ ($\sim$10000 cm^{-1} for the biologically relevant oxygen and nitrogen ligands of non-heme Fe^{II} sites). According to ligand-field (LF) theory, both the $^5T_{2g}$ and ^5E_g states will further split in energy in the low-symmetry environment of non-heme protein active sites dependent upon the coordination number and geometry of the Fe^{II} ligation sphere (Fig. 1).[107–110] For distorted six-coordinate sites, the ^5E_g state will split by up to 2000 cm^{-1} resulting in two LF transitions from the $^5T_{2g}$ ground state to each of the two components of the ^5E_g excited state, centered around $\sim$10000 cm^{-1} and split by $\sim$2000 cm^{-1}. Removal of one ligand produces a square pyramidal five-coordinate site which

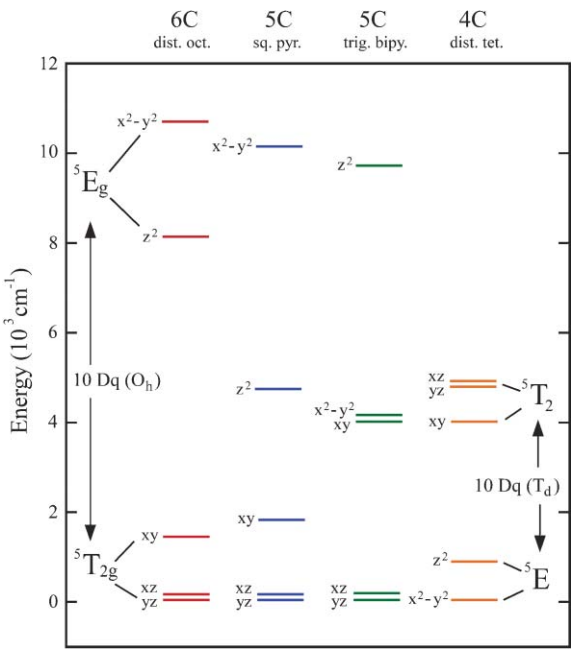

Fig. 1 LF splittings of the Fe^{II} d-orbitals in different ligand environments.

further splits the ^{5}E state, resulting in two LF transitions at $\sim$10000 and $\sim$5000 cm^{-1}. Distortion to a trigonal pyramidal 5C Fe^{II} site changes the LF and lowers the energies of the two LF transitions to $<$10000 cm^{-1} and $<$5000 cm^{-1}. Removal of a second ligand to produce a distorted tetrahedral four-coordinate site results in only low energy LF transitions in the 5000–7000 cm^{-1} region as $10Dq(T_d) \approx -4/9\ 10Dq(O_h)$.

While the splitting of the ^5E_g state can be directly observed using excited state spectroscopy (*i.e.* the near-infrared (NIR) methods described herein), determination of the splitting of the $^5T_{2g}$ ground state is more complex. However, this splitting must be considered as it involves the dπ orbitals and provides key information on π-bonding and backbonding between the Fe^{II} and its ligands. Several factors contribute to the splitting of the $^5T_{2g}$ ground state of the Fe^{II} in a protein environment.[1,111] Spin–orbit coupling (SOC) of the orbital angular momentum associated with the 3-fold orbital degeneracy of the T_{2g} ground state to the $S = 2$ spin state splits the $^5T_{2g}$ state in octahedral symmetry into 7-, 5- and 3-fold degenerate spin–orbit sublevels (Fig. 2, green, λ is the many electron SOC parameter and is ~ -80 cm^{-1} for Fe^{II} in coordination complexes), where the 3-fold degenerate spin–orbit sublevel is lowest in energy. The low-symmetry protein environment of the Fe^{II} ion leads to additional orbital splittings of the $^5T_{2g}$ state, with Δ defining the axial splitting ($\Delta = d_{xz,yz} - d_{xy}$) (Fig. 2, blue) and V the rhombic splitting ($V = d_{xz} - d_{yz}$) (Fig. 2, red) of the dπ orbitals. Combining these SOC and axial/rhombic d orbital splittings leads to the energy diagram for the ground state shown in the expanded scale on the right of Fig. 2. The splitting of the five spin levels ($S = 2$, $M_s = 2,1,0,-1,-2$) of the d_{yz} ground state is called zero-field splitting (ZFS) and as described above derives from the SOC over the low symmetry split $^5T_{2g}$ state. The resulting lowest energy spin doublet in the expanded scale on right is split by an amount δ even in the absence of a magnetic field due to ZFS in less than octahedral symmetry. This ZFS of $\pm M_s$ doublets can only occur for non-Kramers ions, *i.e.* those having an even number of electrons and, thus, integer spins (*e.g.* d^6 with $S = 2$). Application of a magnetic field further splits the doublet (Fig. 2, purple), giving g_{II}. From Fig. 2, both δ and g_{II} depend on Δ and V and on SOC (which is similar for all Fe^{II} sites) and can be utilized to determine Δ and V and, thus, the energy splittings of the three dπ orbitals for a high-spin non-heme Fe^{II} site.

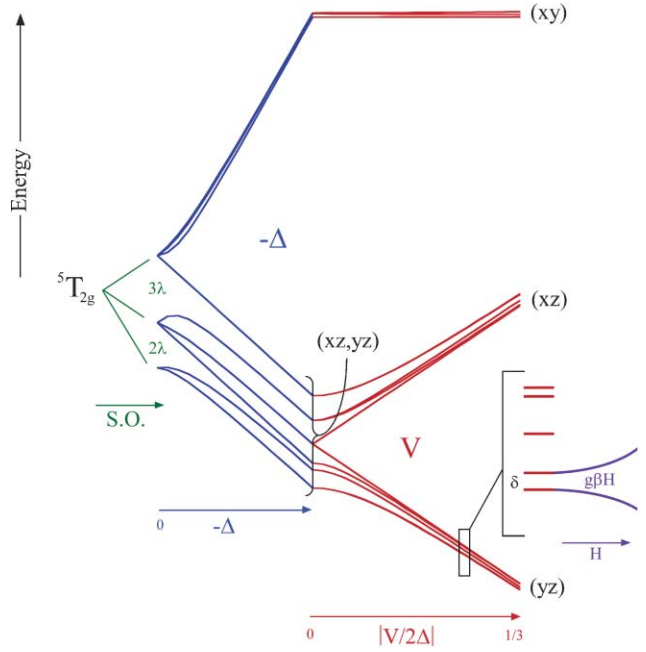

Fig. 2 LF theory of the splitting of the $^5T_{2g}$ ground state of a –ZFS Fe^{II} system.

While the ligand-field splittings of the five d-orbitals of Fe^{II} centers in mononuclear non-heme iron enzymes provide direct information on the geometric and electronic structure of these sites, experimentally determining these splittings had generally been inaccessible. The $^5T_{2g} \rightarrow {}^5E_g$ ligand-field transitions are difficult to observe in absorption as they are parity forbidden d $\rightarrow$ d transitions, exhibiting low extinction coefficients and falling in the near-infrared region where they are obscured by intense contributions from protein and buffer vibrations (in the $<$12000 cm^{-1} region). Furthermore, the $^5T_{2g}$ ground state energy splittings ($<$5000 cm^{-1}) are small relative to the $^5T_{2g} \rightarrow {}^5E_g$ ligand-field transition energies, and traditional methods to probe the ground state such as EPR cannot be utilized as non-Kramers Fe^{II} centers are generally EPR silent due to the ZFS of the lowest spin doublet by δ (Fig. 2, right), which is typically larger than the microwave frequency used in EPR.

We have developed a methodology using a combination of CD and MCD spectroscopies to directly observe the LF transitions of Fe^{II} sites in mononuclear non-heme enzymes due to the different selection rules of these spectroscopies.[1,111] CD and MCD are advantageous for studies of the ligand-field transitions of Fe^{II} sites for several reasons: (1) CD spectroscopy is a differential technique utilizing phase sensitive detection, allowing the routine observation of d $\rightarrow$ d transitions which are magnetic dipole allowed and give CD intensity from systems with extinction coefficients of $\sim$1–10 M^{-1}cm^{-1} and $\Delta\varepsilon$ values of $\sim 10^{-6}$ M^{-1}cm^{-1}, (2) the fact that $\Delta\varepsilon$ is signed allows the resolution of overlapping bands and, in particular, (3) high-spin Fe^{II} ($S = 2$) is paramagnetic and will exhibit a *C*-term MCD signal at low temperature which is 2–3 orders of magnitude more intense than the MCD (and CD) signals associated with the diamagnetic protein background. In addition, we have utilized the magnetic field and temperature dependence of MCD signals (VTVH-MCD) to obtain information about the energy splittings of the Fe^{II} center ground-state sublevels (Fig. 2, expanded scale on right). This provides EPR information from an EPR inactive active site that can then be related to the splitting of the dπ orbitals (Fig. 2).

The LT MCD spectra of 25 structurally defined Fe^{II} model complexes showed excited states consistent with the LF predictions (Fig. 1) as summarized in Fig. 3.[110] Distorted 6C complexes exhibit two transitions centered around 10000 cm^{-1}, split by less than 2000 cm^{-1} (Fig. 3A), square pyramidal 5C complexes exhibit transitions at $>$10000 cm^{-1} and $\sim$5000 cm^{-1}, trigonal bipyramidal 5C sites exhibit transitions at $<$10000 cm^{-1} and $<$5000 cm^{-1} (Fig. 3C) and distorted tetrahedral complexes exhibit only low energy ligand-field transitions (Fig. 3D).

The observed MCD signals of the models show *C*-term MCD behavior, increasing in intensity with decreasing

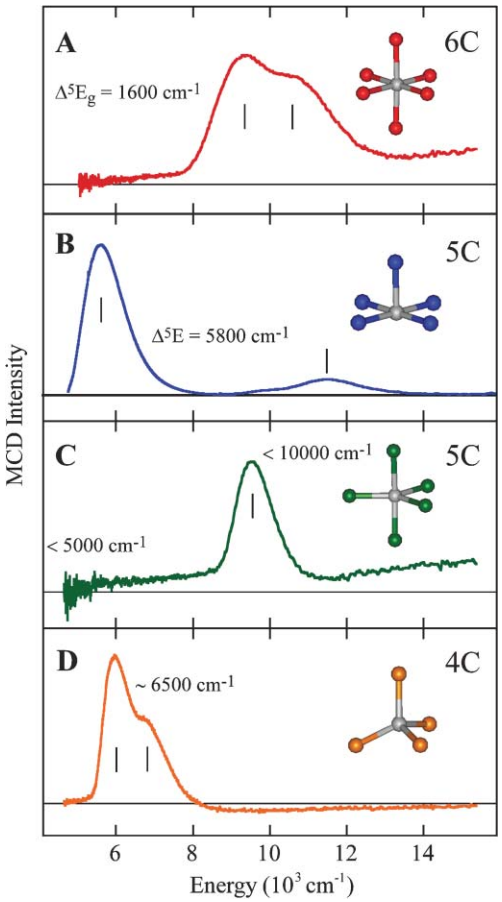

Fig. 3 LT MCD spectra of structurally defined Fe^{II} model complexes. (A) 6C, octahedral $[Fe(H_2O)_6](SiF_6)$, (B) 5C, square pyramidal $[Fe(HB(3,5\text{-}^iPr_2pz)_3)(OAc)]$, (C) 5C, trigonal bipyramidal [Fe(tris(2-(dimethylamino)ethyl)amine)Br]$^+$ and (D) 4C, tetrahedral $[Fe(HB(3,5\text{-}^iPr_2pz)_3)(Cl)$.

temperature and increasing magnetic field (Fig. 4A).[107,111,112] Importantly, the temperature and field dependence of non-Kramers Fe^{II} centers is characterized by a set of nested saturation magnetization curves (*i.e.* non-superimposable isotherms when plotted as a function of $\beta H/2kT$ (Fig. 4B)). This contrasts the saturation magnetization behavior observed for a Kramers $S = 1/2$ ion where all isotherms superimpose. The nesting of non-heme Fe^{II} sites directly reflects the ZFS of the ground state by δ (Fig. 2, inset). The ground-state spin Hamiltonian parameters (δ, g_{II}) for a given Fe^{II} site can be derived from numerical fitting of the observed saturation magnetization behavior as described in ref. 107. Thus, an excited state is used to obtain EPR parameters for an EPR non-detectable ground state. The ground-state δ and g_{II} extracted from VTVH-MCD can be used to directly obtain the ligand-field splitting of the $^5T_{2g}$ state (Δ and V in Fig. 2) and, therefore, the t_{2g} d-orbital energies. As these d-orbitals are involved in π-donor/acceptor interactions, analysis of their splitting provides insight into the nature of the bonding with the ligand environment.

Combined, the NIR CD, MCD and VTVH-MCD spectroscopies determine the energy splitting of the five d-orbitals of the metal site as described above, providing detailed geometric and electronic descriptions of the active sites in the mononuclear non-heme iron enzymes. This methodology can be used to probe the resting Fe^{II} site, its interactions with cofactor and substrate, and its oxygen reactivity to obtain molecular level insight into catalysis.

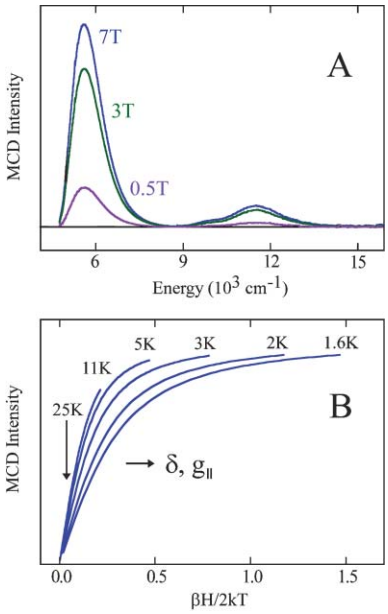

Fig. 4 (A) Field dependence and (B) saturation behavior of an $S = 2$ non-Kramers Fe^{II} complex.

III. Structure–function correlations

A. O_2 activation

While the uncatalyzed reactions of dioxygen with organic substrates are thermodynamically favorable, they are kinetically slow as these reactions are spin forbidden and the one electron redox potential of dioxygen is low. The classes of mononuclear non-heme iron enzymes in Table 1B activate dioxygen for catalysis using high-spin Fe^{II} active sites.[1] To achieve oxygen activation, these systems utilize additional reducing equivalents which derive from one of two sources: (1) redox active cofactors or (2) redox active substrates. Application of the Fe^{II} methodology outlined in II to enzymes using either redox active cofactors or substrates has provided insight into the active site structure requirements in these different classes and defined general mechanistic strategies for efficient oxygen activation in the mononuclear non-heme iron enzymes.

(1) O_2 activation: enzymes with redox active cofactors. Many mononuclear non-heme iron enzymes utilize redox active cofactors to supply additional reducing equivalents to activate dioxygen, including the α-KG-dependent dioxygenases, pterin-dependent hydroxylases and Rieske dioxygenases. It is important in these systems to understand how oxygen activation is controlled at a molecular level to ensure coupled *vs.* uncoupled oxidation of cofactor and substrate. Applications of the Fe^{II} methodology to phenylalanine hydroxylase, a pterin-dependent hydroxylase, clavaminate

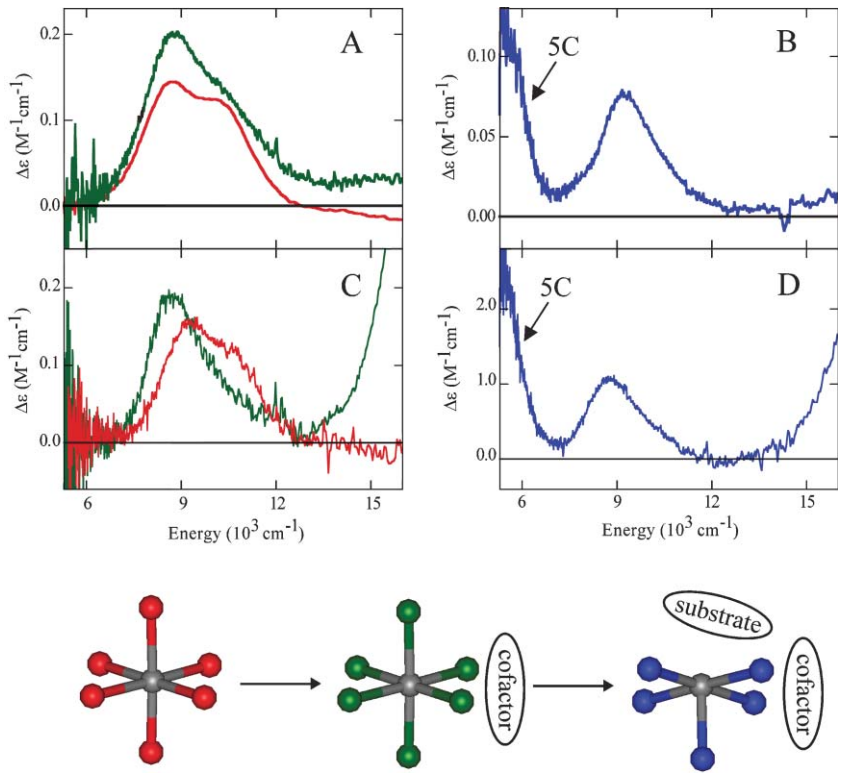

Fig. 5 LT MCD spectra (top) of (A) resting PAH^T (red) and PAH/Fe^{II}/5-deaza-6-MPH_4 (green), (B) PAH/Fe^{II}/5-deaza-6-MPH_4/L-Phe, (C) resting CS2 (red) and $CS2/Fe^{II}$/α-KG (green) and (D) $CS2/Fe^{II}$/α-KG/DGPC where DGPC is the substrate for the hydroxylation reaction of CS2. Scheme of O_2 activation with redox active cofactors (bottom).

synthase, an α-KG dependent dioxygenase, and pthalate dioxygenase, a Rieske dioxygenase, have provided detailed insight into the mechanism of dioxygen activation by redox active cofactor utilizing enzymes.

The MCD spectrum of resting PAH contains two LF transitions at 8500 and 10300 cm^{-1} (*i.e.* $\Delta^5E_g < 2000$ cm^{-1}), indicative of a distorted 6C site (Fig. 5A, red).[52] Binding of the non-redox active pterin analog, 5-deaza-6-methyltetrahydropterin (5-deaza-6-MPH_4) does not alter the geometric or electronic structure of the resting site, as it remains 6C with LF transitions at 8500 and 10100 cm^{-1} (Fig. 5A, green).[53] Additionally, binding of substrate L-Phe to resting PAH has little effect on the Fe^{II} active site as it remains 6C from the observed LF transitions in MCD. In contrast, simultaneous binding of both substrate and cofactor leads to a dramatic change in the MCD spectrum indicating a large slitting of the ^5E excited state with an intense low energy LF transition at <5000 cm^{-1} and a second transition at 9280 cm^{-1} (Fig. 5B).[53] This excited state splitting is indicative of a 5C site. VTVH-MCD data also show a large change in nesting which gives a larger splitting of the $^5T_{2g}$ ground state, consistent with the presence of a 5C site. Thus, simultaneous binding of substrate and pterin cofactor leads to a 6C → 5C conversion of the Fe^{II} active site (Fig. 5, bottom), opening up a coordination position for reaction with O_2 when all the necessary reducing equivalents for oxygen activation are present (*i.e.* substrate and pterin in PAH).

MCD studies of CS2 and PDO have shown the same 6C → 5C conversion upon substrate (and α-KG cofactor for CS2) binding. This appears to be a general mechanistic strategy for O_2 activation in enzymes utilizing redox active cofactors. CS2 contains LF transitions in the MCD consistent with a distorted 6C Fe^{II} site for both the resting and α-KG bound complexes (Fig. 5C, red).[71] In contrast to PAH, binding of cofactor (α-KG) to CS2 produces a significant change in the MCD spectrum (Fig. 5C, green) due to bidentate coordination of α-KG to Fe^{II} as determined from analysis of the MLCT transitions (the intense MCD signal at >15000 cm^{-1} in Fig. 5C, green) and the large $^5T_{2g}$ ground state splitting obtained from the VTVH-MCD in ref. 71, which are consistent with π-backbonding between the Fe^{II} dπ orbitals and α-KG. While CS2 catalyzes three different reactions (*i.e.* hydroxylation, ring closure and desaturation) depending upon substrate, binding of any of these substrates in the absence of α-KG cofactor results in little perturbation to resting CS2 as all are distorted 6C sites.[73] In contrast, binding of both α-KG and each of these substrates was found to convert the Fe^{II} site to 5C as evidenced by new low-energy (<5000 cm^{-1}) features in the MCD (Fig. 5D). VTVH-MCD data of the $CS2/Fe^{II}$/α-KG/substrate complexes indicate a large splitting of the Fe^{II} dπ orbitals and, combined with analysis of the MLCT transitions observed, require that the α-KG cofactor remains bound in a bidentate fashion upon substrate binding.

Phthalate dioxygenase is different in that a second redox center is utilized, a Rieske cluster, which is covalently attached to the protein and supplies an additional reducing equivalent for oxygen activation. The MCD spectrum of resting PDO contains two ligand-field transitions centered at ~9700 cm^{-1}

and split by ~1700 cm^{-1}, indicating a distorted 6C resting site.[87,88] Binding of substrate, phthalate, leads to a low energy Fe^{II} transition in the MCD spectrum. Analysis of the spectrum showed that the substrate bound complex was a mixture of square pyramidal and trigonal bipyramidal 5C Fe^{II} sites.

The general mechanistic strategy outlined above appears to be key to the proper functioning of mononuclear non-heme iron enzymes that utilize redox-active cofactors such as pterin, α-KG and covalently bound Rieske clusters to activate dioxygen for reaction with organic substrates. For these systems, the Fe^{II} active sites with bound substrate or cofactor are generally 6C until the co-substrate also binds to prevent any uncoupled reaction involving the two (or greater) electron reduction of O_2. Such an uncoupled reaction would lead to the generation of peroxy-Fe^{III} or Fe^{IV} species in the absence of substrate and result in autoxidation of the site. However, the generation of a 5C site upon binding of both cofactor and substrate facilitates the dioxygen reaction when all the components are present for the coupled reaction. Thus, nature has developed an elegant strategy for efficient oxygen activation to ensure coupled oxidation between substrates and cofactors only when all the necessary components for the reaction are present.

(2) O_2 activation: redox active substrates. While a general mechanistic strategy has been defined for mononuclear non-heme iron enzymes that utilize redox-active cofactors to activate dioxygen for reaction with organic substrates, several enzymes exist which, instead, utilize redox-active substrates which themselves supply all the necessary reducing equivalents for oxygen activation. These include the extradiol dioxygenases which utilize catechol substrates,[33] a sub-class of α-KG-dependent dioxygenases which have the α-keto acid cofactor covalently linked to the substrate (*i.e.* HPPD[81] and HmaS[82]) and IPNS, which has high sequence homology to the α-KG enzymes and utilizes the redox-active substrate ACV to catalyze a four electron double ring closure reaction.[83] To define the approach to oxygen activation in enzymes which use substrates which themselves contain all the necessary reducing equivalents for the oxygen reaction, the Fe^{II} methodology has been applied to the extradiol dioxygenases catechol 2,3-dioxygenase and 2,3-dihydroxybiphenyl 1,2-dioxygenase (DHBD) and the α-KG-dependent dioxygenases HPPD and HmaS.

The MCD spectrum of resting DHBD consists of two ligand-field transitions at 5500 and 11000 cm^{-1}, indicative of a square pyramidal 5C site (Fig. 6A, red).[40] Binding of substrate, 2,3-dihydroxybiphenyl, results in a new square pyramidal 5C site with ligand-field transitions at 6000 and 10500 cm^{-1} (Fig. 6A, blue). Thus, in contrast to the cofactor dependent enzymes in IIIA-1, DHBD is 5C in both the resting and substrate-bound forms. This coordination difference of resting DHBD relative to CS2 and PAH is the lack of a water ligand in the sixth coordination position. Possible structural contributions to this water coordination difference include: (1) steric hindrance by the hydroxyl group of the Tyr250 residue in the vicinity of the open position in DHBD compared to the more open protein pockets in PAH and the α-KG dioxygenases and (2) the lack of the internal H-bond to a water ligand from the monodentate coordinated carboxylate ligand

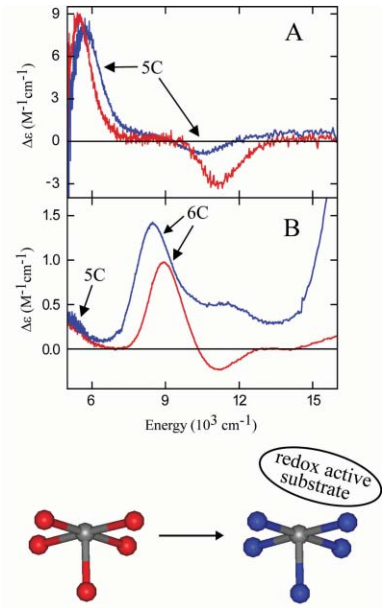

Fig. 6 LT MCD (top) of (A) resting DHBD (red) and DHBD/Fe^{II}/DHB (blue) and (B) resting HPPD (red) and HPPD/Fe^{II}/HPP (blue). Scheme of O_2 activation with redox active substrates (bottom).

present in both PAH and the α-KG dioxygenases. The 5C resting site in DHBD reacts only very slowly with O_2 as the one electron reduction of O_2 is unfavorable due to its low redox potential and the formation of an Fe^{III} superoxide species with a weak Fe^{III}–O_2^- bond.[40] In contrast, the 5C substrate-bound species is very reactive towards O_2 as all the reducing equivalents required for oxygen activation are now present.

A sub-class of α-KG-dependent dioxygenases which have an α-keto acid moiety covalently linked to the substrate are analogous to the extradiol dioxygenases, as the substrates themselves carry all the necessary reducing equivalents for oxygen activation. MCD studies of one member of this sub-class, HPPD, showed at least three d → d transitions (Fig. 6B, red) which requires the presence of more than one Fe^{II} site since LF theory dictates that no single site can exhibit more than two transitions in this energy region.[113] Due to the presence of a low energy transition at <5000 cm^{-1} and at least two transitions in the 10000 cm^{-1} region, this mixture was determined to consist of distinct 5C and 6C Fe^{II} sites. While resting DHBD is purely 5C, resting HPPD is predominately 6C likely due to the lack of the steric interaction of a nearby Tyr residue in HPPD.[114] Binding of HPP substrate results in a different MCD spectrum with at least three LF transitions (Fig. 6B, blue), indicative of a new mixture of 5C and 6C Fe^{II} sites with bidentate coordination of the α-keto acid moiety of HPP to Fe^{II} as determined from analysis of the MLCT transitions (at >15000 cm^{-1}) and the $^5T_{2g}$ ground state splitting determined from the VTVH-MCD data. In contrast to CS2, substrate binding does not significantly perturb the amount of 5C present, likely due to conformation restrictions of having the substrate and cofactor covalently linked. Only the substrate-bound form of HPPD is highly reactive towards O_2 as the one electron reduction of O_2 by the 5C component of resting HPPD is unfavorable as previously discussed above for

DHBD, where the bound substrate provides the additional reducing equivalents for O_2 reactivity.

MCD studies of HmaS, which utilizes the same substrate as HPPD but carries out a different reaction, have also shown that the resting Fe^{II} site is predominately 6C.[115] Binding of substrate results in a mixture of distinct 5C and 6C species with bidentate coordination of the α-keto acid moiety of HPP to Fe^{II} in a bidentate fashion, analogous to the results for HPPD. In addition, EXAFS[116,117] and crystallographic studies[47,48] of IPNS, have shown a 6C resting site (Mn^{II} substituted for the resting site crystal structure) which is converted to a 5C species upon substrate (ACV) binding.

These studies of mononuclear non-heme iron enzymes that utilize redox active substrates to activate dioxygen show that the resting Fe^{II} active sites can be either 5C or 6C. While the presence of a 5C resting site for enzymes which use redox active cofactors to activate dioxygen would be problematic due to the possibility of uncoupled oxidation of cofactor in the absence of substrate, this is not a problem for enzymes utilizing redox active substrates as the 5C resting site reacts only very slowly with O_2. In contrast, the substrate bound complexes of enzymes utilizing redox active substrates all contain 5C sites (purely 5C or a mixture of 5C and 6C species) which are highly reactive towards O_2 as an open coordination position is present and all the reducing equivalents for oxygen activation are now available. Thus, the resting sites of these enzymes can be 5C, 6C or a mixture thereof and studies of these enzymes show that all are utilized. The presence of a 5C Fe^{II} species upon substrate binding with one open coordination position to bind and activate dioxygen (Fig. 6, bottom) appears to be a mechanistic requirement for oxygen activation with redox active substrates.

B. Active site structural insight into reactivity

Following the activation of dioxygen by mononuclear non-heme iron enzymes, the resulting iron-oxygen intermediates react with substrates to yield the desired products. Within systems that utilize the same general mechanism for oxygen activation (*i.e.* redox active cofactors or redox active substrates), the type of reactivity exhibited varies and includes aliphatic hydroxylation, aromatic electrophilic hydroxylation, oxidative ring closure and desaturation. The Fe^{II} methodology was applied to systems with different reactivities in which (1) a single enzyme exhibits different reactivites (aliphatic hydroxylation *vs.* desaturation) depending on substrate and (2) similar enzymes which exhibit different reactivates (benzylic *vs.* aromatic hydroxylation) towards a conserved substrate. These studies defined active site structural differences which correlate with these different reactivities.

(1) Hydroxylation *vs.* desaturation. As discussed in IIIA-1, CS2 is an α-KG dependent dioxygenase which is capable of catalyzing three different reactions with a single Fe^{II} site depending upon substrate in the biosynthesis of the potent β-lactamase inhibitor, clavulanic acid (Scheme 1).[64,118] In the first step, CS2 catalyzes the hydroxylation of deoxyguanidinoproclavaminic acid (DGPC) to guanidinoproclavaminic

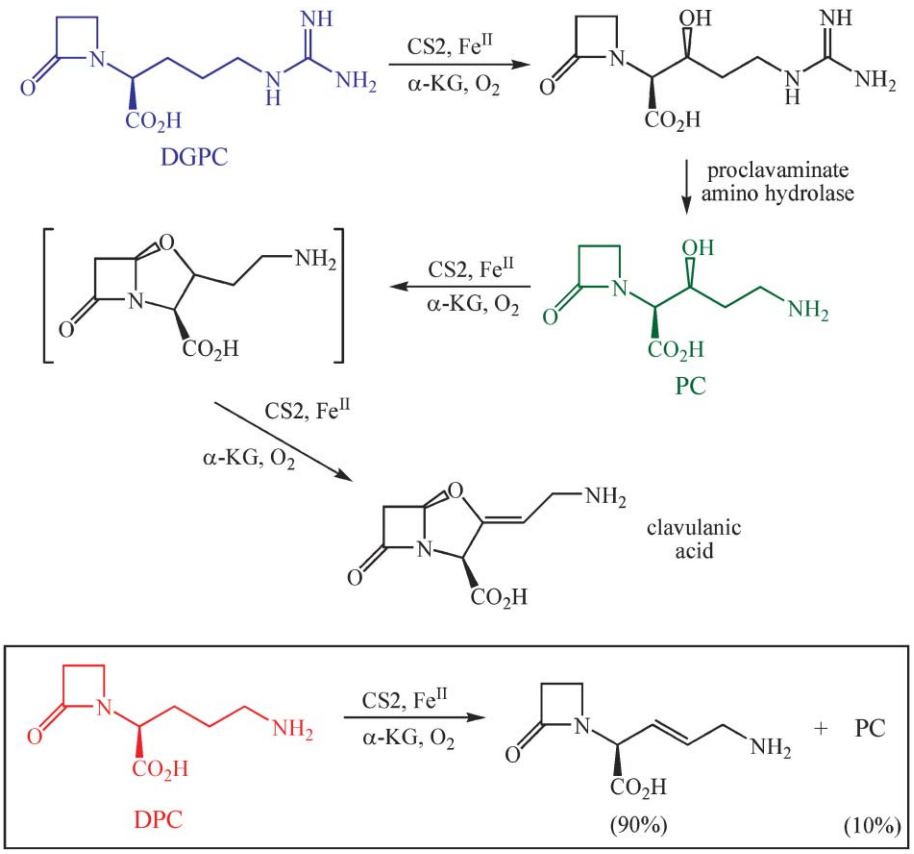

Scheme 1 Reactions catalyzed by CS2.

acid. Following conversion of guanidinoproclavaminic acid to proclavaminic acid (PC) by proclavaminate amidino hydrolase,[119,120] CS2 catalyzes the oxidative ring closure of PC and its subsequent desaturation to produce clavulanic acid. Studies have also shown that CS2 catalyzes the conversion of the substrate analog deoxyproclavaminic acid (DPC) to a major desaturation product and a minor hydroxylation product, indicating that DPC is a reasonable analog for desaturation of the biological substrate.[121]

To determine the geometric and electronic structure of the Fe^{II} active sites that react with dioxygen to yield product and to correlate these to the different reactivities observed, the Fe^{II} methodology was applied to the quaternary complexes of CS2 with Fe^{II}, α-KG and substrate bound for each type of reaction (DGPC for hydroxylation, PC for oxidative ring closure and DPC for desaturation).[72,73] The MCD spectra for all three substrates (Fig. 7, top, for DGPC and DPC) show a band at $<5000\ cm^{-1}$ indicative of a 5C species and additional LF transitions in $10000\ cm^{-1}$ region indicative of a 6C component. Each substrate bound form was found to contain a different composition of 5C and 6C species by analysis of the intensity of the low energy 5C transition, with the DGPC complex containing the most 5C (Fig. 7, blue, band intensity at $<5000\ cm^{-1}$) and the DPC complex containing the smallest 5C component (Fig. 7, red, reduced band intensity at $<5000\ cm^{-1}$).

These observed differences in the MCD spectra for the quaternary complexes reflect structural differences that can be correlated to differences in reactivity. The generally considered mechanisms for the reactions of α-KG dioxygenases invoke an

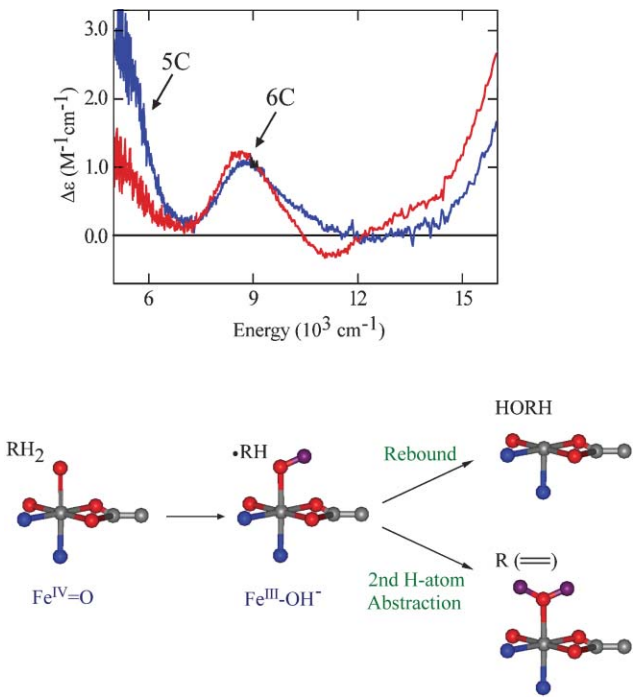

Fig. 7 LT MCD (top) of CS2/Fe^{II}/α-KG/DPC (red) and CS2/Fe^{II}/α-KG/DGPC (blue). The CS2/Fe^{II}/α-KG/PC spectrum is not shown. Scheme of the reaction pathways for hydroxylation *vs.* desaturation (bottom).

Fe^{IV}=O species (see Section IV) resulting from nucleophilic attack of activated O_2 on the α-keto group of α-KG yielding decarboxylation. For the three possible reactions of CS2, the Fe^{IV}=O would initially abstract a hydrogen atom from a C–H bond of the substrate (RH_2) to generate a substrate radical ($HR^{\cdot}$) and an Fe^{III}–OH^- species (Fig. 7, bottom). Hydroxylation reactions would involve a rebound step requiring the homolytic cleavage of the Fe^{III}–OH^- bond to yield a 5C Fe^{II} site and a hydroxyl radical which combines with the substrate radical to yield the hydroxylation product (HORH). By contrast, desaturation and oxidative ring closure reactions would involve a second H-atom abstraction by the Fe^{III}–OH^- species, yielding a water coordinated 6C Fe^{II} species and a substrate diradical ($R^{\cdot\cdot}$) which forms either a double bound or a ring.

Consideration of the energies of formation of the products for hydroxylation (the hydroxylated product plus a 5C Fe^{II} site) and desaturation (desaturation product plus a 6C Fe^{II}–OH_2 site) provides a basis for evaluating the ability of the Fe^{III} hydroxide species to carry out a rebound reaction leading to hydroxylation *vs.* a second H-atom abstraction reaction leading to desaturation or ring closure. As the strength of the water bond to the Fe^{II} site increases, the abstraction of a second H-atom to form such a site becomes more favorable. Therefore, it was postulated that CS2 could contribute to the reactivities of the Fe^{III}–OH^- species by regulating the energy of the water–Fe^{II}_{5C} bond in the enzyme–product complex.

From the MCD studies of the CS2/Fe^{II}/αKG/substrate complexes which showed a mixture of 5C and 6C species (where an extra water ligand is present in the 6C sites), the smallest amount of the 5C component was observed with the substrate DPC, which undergoes a desaturation reaction (Fig. 7, red). In contrast, the DGPC substrate, which undergoes a hydroxylation reaction, contained the largest amount of the 5C component (Fig. 7, blue), consistent with a low value of the water–Fe^{II}_{5C} interaction energy. Therefore, the observed MCD data are consistent with a model in which CS2 controls hydroxylation *vs.* desaturation reactivities by modulating the affinity of water for the Fe^{II} site.

(2) H-atom abstraction *vs.* electrophilic attack. The α-KG-dependent dioxygenases generally perform substrate hydroxylation through a reaction pathway involving H-atom abstraction by an iron-oxygen intermediate (*e.g.* prolyl hydroxylase, TauD, asparagine hydroxylase). Recent spectroscopic studies of a trapped intermediate in TauD support the identification of the iron-oxygen intermediate for this reaction, which involves H-atom abstraction, to be an Fe^{IV}=O species.[78–80] The α-keto acid dependent dioxygenases HPPD and HmaS are particularly interesting in that they use the same substrate (HPP), to catalyze two different reactions (Scheme 2): HPPD catalyzes aromatic hydroxylation to yield homogentisate (HG)[81] and HmaS catalyzes benzylic hydroxylation to form (*S*)-4-hydroxymandelate (HMA).[82] The intermediate of HmaS is likely similar to TauD as both perform H-atom abstraction, however, HPPD is different in that the aromatic hydroxylation reaction catalyzed is proposed to involve electrophilic attack by an iron-oxygen intermediate. While electrophilic attack on an aromatic ring has also been observed

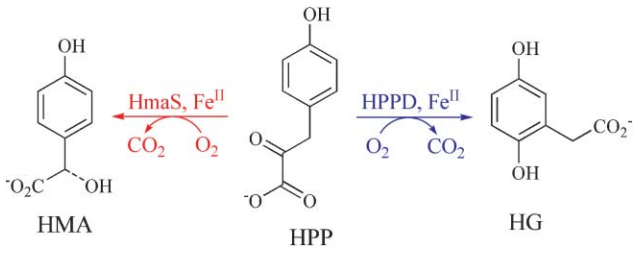

Scheme 2 Reactions catalyzed by HPPD and HmaS.

in the pterin-dependent hydroxylases, the reactive iron-oxygen intermediate has not been identified.[59]

Using CD and MCD, direct comparison of the spectra of HPPD and HmaS provided insight into the active site geometric and electronic contributions which determine the differential reactivity of related enzymes to a conserved substrate.[113,115] Focusing on the substrate-bound forms of the enzymes which are highly reactive to O_2, the MCD spectra of HPP-bound HPPD (Fig. 8, blue) and HPP-bound HmaS (Fig. 8, red) are very similar. Both complexes exhibit at least three LF transitions at similar energies in the 8000–12000 cm^{-1} region, requiring the presence of at least two distinct Fe^{II} sites as LF theory dictates that no single Fe^{II} site can exhibit more than two transitions in this energy region (see methodology). The observed low energy transition at <5000 cm^{-1} in HPPD/Fe^{II}/HPP combined with VTVH-MCD data on both complexes indicate that a 5C site is one component of the mixture, while the additional LF transitions in the 10000 cm^{-1} region can be correlated to a 6C component. Analysis of the MLCT transitions (at >15000 cm^{-1}) and the large $^5T_{2g}$ splitting determined from the VTVH-MCD data indicate that the α-keto acid moiety of HPP is bound in a bidentate mode to Fe^{II} in both complexes. While the MCD data on HPPD and HmaS indicated substrate-bound complexes which are very similar, limited differences are observed, importantly inversion of the sign in CD, which suggests a different local environment (*i.e.* substrate conformation) around the Fe^{II} sites.

As the spectroscopic comparison of HPPD and HmaS suggested very similar substrate-bound species, activation of dioxygen and subsequent decarboxylation should follow parallel reaction pathways to generate similar iron-oxygen intermediates. Therefore, the differences in reactivities observed in these enzymes (H-atom abstraction *vs.* electrophilic attack) do not appear to arise from differences in the iron-oxygen intermediate generated along the reaction pathway. The inversion of sign observed in the CD spectra of substrate-bound HPPD and HmaS strongly suggested different substrate conformations in these enzymes. Therefore, it was proposed that the differences in reactivity of HPPD and HmaS may relate to differences in the protein pockets of the two enzymes which would lead to different interactions of the decarboxylated substrate with the iron-oxygen intermediate. The results with TauD suggest that the iron-oxygen intermediate generated in HmaS should be an Fe^{IV}=O species to perform H-atom abstraction, therefore, decarboxylation of HPPD would similarly generate an Fe^{IV}=O intermediate. Frontier molecular orbital analysis of an Fe^{IV}=O model structure with a coordinated, decarboxylated substrate was utilized to evaluate this possibility. Frontier orbitals with good overlap of the substrate HOMO with the Fe^{IV}=O LUMO could be obtained for either H-atom abstraction (Fig. 8, left) from the benzylic position (HmaS) or electrophilic attack (Fig. 8, right) on the aromatic ring (HPPD) by rotation of the substrate around the $C_{Carbonyl}$–$C_{Benzylic}$ and $C_{Benzylic}$–$C_{Aromatic}$ bonds. Since the H-atom abstraction conformation was only ~1 kcal mol^{-1} lower in energy than that for electrophilic attack and both were 7–8 kcal mol^{-1} higher in energy than the optimized conformation, both conformations would be readily accessible to the enzymes through non-covalent interactions with the substrate. Therefore, CD and MCD studies of HPPD and HmaS coupled to FMO analysis indicate that very similar Fe^{IV}=O species can perform either H-atom abstraction or electrophilic attack with control of the substrate orientation by the protein pocket determining reactivity.

C. CO_2 activation of ACCO

The structure–function correlations in the mononuclear non-heme enzymes presented above have described systems utilizing only substrate and cofactors (when required) for oxygen activation and substrate transformation. 1-Aminocyclopropane-1-carboxylic acid oxidase (ACCO), an α-KG related enzyme that catalyzes the last step in the biosynthesis of the plant hormone, ethylene,[84,85] is different in that the coupled oxidation of substrate, 1-aminocyclopropane-1-carboxylic acid (ACC), to the oxidation of the cosubstrate ascorbate, requires the additional activator molecule CO_2 in order to achieve continuous turnover.[122,123] Application of the

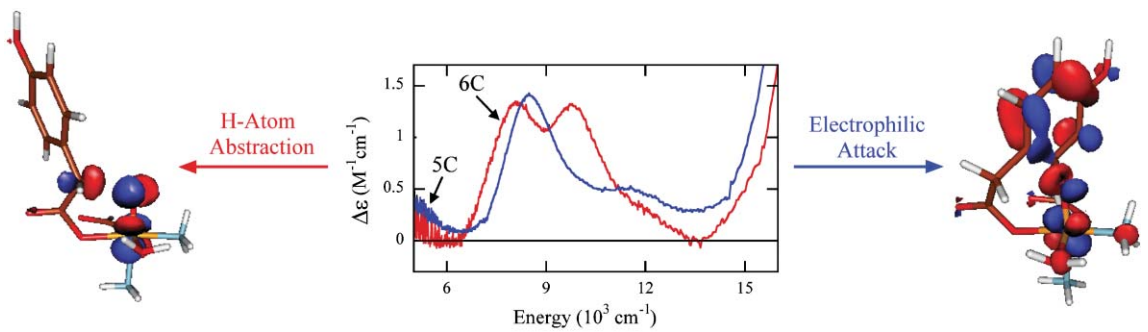

Fig. 8 LT MCD of HPPD/Fe^{II}/HPP (blue) and HmaS/Fe^{II}/HPP (red) and the substrate orientations for FMO overlap for their corresponding reactivities with an Fe^{IV}=O intermediate: H-atom abstraction and electrophilic attack.

Fe^{II} methodology to ACCO provided insight into the mechanism of oxygen activation in ACCO and defined the nature of the CO_2 activation on a molecular level.

The MCD spectra of resting ACCO, ACCO/Fe^{II}/ascorbate and ACCO/Fe^{II}/CO_2 all exhibited only two LF transitions centered around $\sim$10000 cm^{-1} and split by $\sim$2000 cm^{-1}, indicating disorted 6C Fe^{II} sites.[124] Thus, these complexes are coordinatively saturated, preventing reaction with dioxygen. Binding of substrate ACC to resting ACCO results in an MCD spectrum with at least three LF transitions (Fig. 9A, red), indicating a mixture of Fe^{II} sites. Based upon ENDOR and EPR studies on the ACCO/Fe^{II}/ACC/NO complex, ACC likely binds to the Fe^{II} center in a bidentate mode through its 1-amino and 1-carboxylate groups.[125] Importantly, the presence of a low energy MCD transition at $<$5000 cm^{-1} (Fig. 9A, red) indicates that a 5C Fe^{II} site is one component of the mixture. The presence of a 5C component with an open coordination position upon ACC binding in the absence of cofactor allows for an uncoupled oxidation reaction, which would result in enzyme inactivation.

Addition of the activator CO_2 to the ACCO/Fe^{II}/ACC complex suppresses the low energy transition associated with the 5C species and, thus, the site remains purely 6C (Fig. 9A, blue), thereby preventing oxygen binding and uncoupled oxidation. From the MCD spectra of ACCO/Fe^{II}/ACC/CO_2 plus ascorbate, addition of cofactor generates a 5C species as indicated by the presence of a low energy ($<$5000 cm^{-1}) LF transition (Fig. 9B, purple), which is also present upon ascorbate binding in the absence of CO_2 (Fig. 9B, green). As

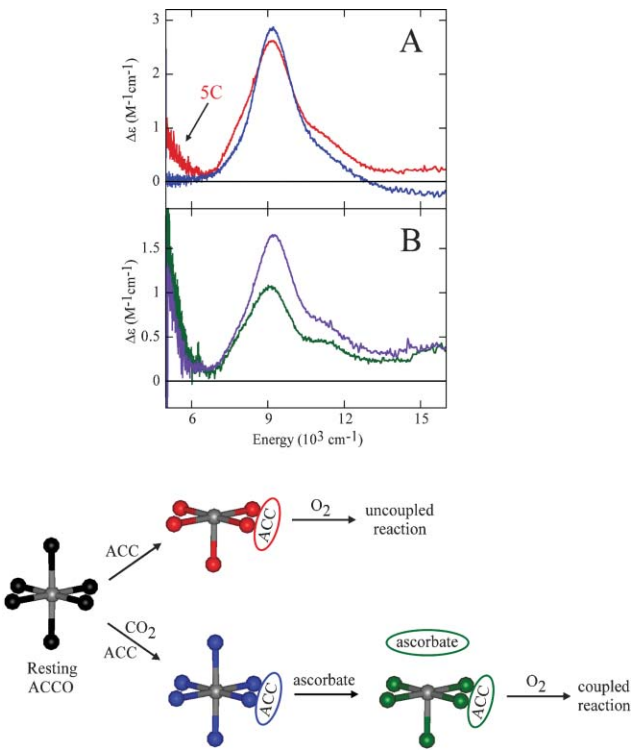

Fig. 9 MCD spectra of ACCO (top). (A) MCD of ACCO/Fe^{II}/ACC (red) and ACCO/Fe^{II}/ACC/CO_2 (blue) and (B) MCD of ACCO/Fe^{II}/ACC/ascorbate (green) and ACCO/Fe^{II}/ACC/CO_2/ascorbate (purple). Scheme of O_2 activation and the role of CO_2 (bottom).

both the substrate and cofactor are present, the coordination unsaturation of the 5C Fe^{II} species allows for oxygen activation and coupled oxidation.

Based upon these MCD studies, a model for oxygen activation and the nature of the CO_2 activation was determined (Fig. 9, bottom). While resting ACCO is 6C, binding of substrate ACC in the absence of CO_2 and cofactor results in a 5C site that can undergo an uncoupled oxidation to inactivate the enzyme. However, when CO_2 is present the general mechanistic strategy for oxygen activation with redox-active cofactors (section IIIA-1) is conserved as the Fe^{II} site is 6C and unreactive towards O_2. Binding of ascorbate cofactor to ACCO/Fe^{II}/ACC/CO_2 produces a 5C Fe^{II} active site with an open coordination position, allowing for oxygen activation and coupled oxidation to yield product. Thus, ACCO utilizes a small molecule activator to stabilize coordination to the sixth ligand site in the substrate bound complex and allow for a 5C Fe^{II} site only when both substrate and cofactor are bound.

While it is clear that CO_2 plays a major role in protecting ACCO from uncoupled oxidation when only ACC is bound, the molecular mechanism of the interaction of CO_2 with the Fe^{II} active site is unresolved. As the coordinated water ligand of the ACCO/Fe^{II} complex should have a pK_a $\sim$9.5,[126] one possible model involves the nucleophilic attack of a coordinated hydroxide group on the carbon of CO_2 at neutral pH to form a bicarbonate ligand. Electrostatic interaction of the resulting bicarbonate with a nearby C-terminal arginine group, conserved in all known ACCO enzymes, could provide further stabilization. An alternative possible model involves binding of CO_2 to Fe^{II} in a linear, non-hydrated form as suggested by crystallographic studies of CO_2 binding in the DAOCS/Fe^{II}/succinate/CO_2 complex.[127]

D. Bleomycin binding to DNA

While the vast majority of mononuclear non-heme iron enzymes utilize substrates which are small molecules, a few utilize substrates which are biological macromolecules. Examples include AlkB which is an α-KG-dependent dioxygenase which repairs DNA methylation lesions[67–69] and asparagine hydroxylase which hydroxylates a specific asparagine residue in the hypoxia inducible factor (HIF) 1-α protein to regulate response to hypoxic conditions.[77,128] A well-studied example is bleomycin, a histidine glycopeptide antibiotic capable of catalyzing both single- and double-strand DNA cleavage in the presence of metal ions (in particular, Fe^{II}) and dioxygen.[96,97,129] Application of the Fe^{II} methodology to BLM has provided insight into the geometric and electronic structure of the resting Fe^{II} site and the effects of DNA binding.

While no crystal structure is available for BLM/Fe^{II}, the MCD spectrum (Fig. 10, blue) of this species contained two LF transitions at 9400 and 12050 cm^{-1}, indicative of a 6C resting Fe^{II} site.[100] The large value of Δ^5E_g observed (2650 cm^{-1}) indicated the presence of one weak axial ligand. However, controversy existed over the nature of the six ligands of BLM to Fe^{II}. While four equatorial ligands are generally accepted to derive from the pyrimidine, imidiazole, deprotonated amide and secondary amine of the β-aminoalanine

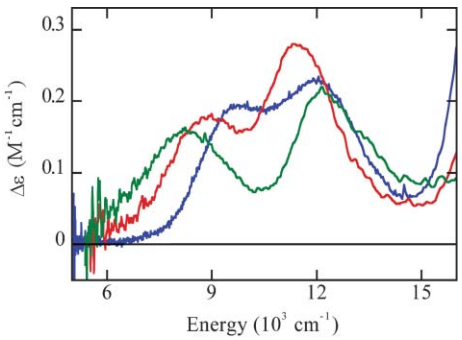

Fig. 10 MCD spectra of BLM/Fe^{II} (blue) and the derivatives *iso*-PEPLM/Fe^{II} (red) and (DP)-PEPLM/Fe^{II} (green).

fragment (Fig. 11, blue atoms), possible axial ligation of the primary amine of the β-aminoalanine (Fig. 11, green) and/or the carbamoyl substituent on the mannose sugar (Fig. 11, red).[1] To evaluate ligation by these residues, MCD studies on the BLM derivatives *iso*-peplomycin (*iso*-PEPLM) (PEPLM is the same as BLM except for the bithiazole tail region, Fig. 11), where the carbamoyl substituent of PEPLM is shifted from the 3- to the 2-hydroxyl group of the mannose sugar, and depyruvamide (DP)-PEPLM, where the β-aminoalanine fragment is replaced by an H atom removing the primary amine).[101] Both derivatives showed significant perturbations in their MCD spectra compared to BLM/Fe^{II} (Fig. 10) and, hence, distorted coordination environments relative to resting BLM, consistent with direct coordination of both the the primary amine of the β-aminoalanine and the 3-*O*-carbamoyl substituent. Coordination of the 3-*O*-carbamoyl residue was

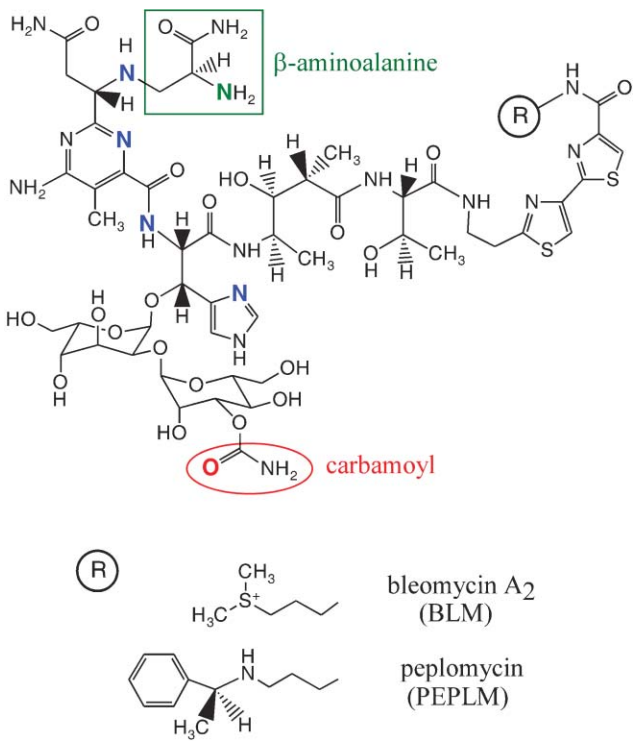

Fig. 11 BLM ligand structure. Colored atoms indicate proposed ligation residue to Fe^{II}.

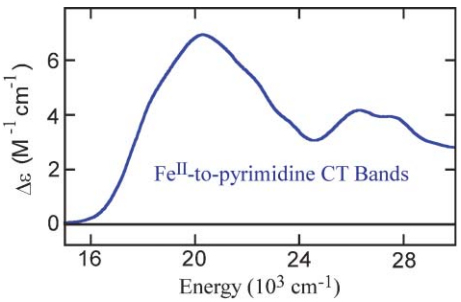

Fig. 12 UV/Vis MCD spectrum of BLM/Fe^{II} showing the MLCT transitions.

also found to account for the weak axial ligand identified from the MCD of BLM/Fe^{II}.

A key deviation from non-heme Fe^{II} enzymes was the presence of low energy MLCT transitions (Fig. 12), due to back-bonding between Fe^{II} and a pyrimidine ligand in the equatorial plane of the BLM.[100] The presence of backbonding contributes to the reversible binding of O_2 by BLM/Fe^{II}, decreasing the extent of charge transfer to O_2 and, thus, decreasing the likelihood of O_2^- dissociation. This reduced charge transfer also promotes further reduction of the site to form activated bleomycin (Fe^{III}–OOH). While the presence of low energy MLCT transitions, the reversibility of O_2 binding and the formation of low-spin complexes with CO and NO observed for BLM/Fe^{II} more closely parallel heme than non-heme chemistry, heme systems exhibit much greater back-bonding. Thus, BLM/Fe^{II} appears to be intermediate between heme and non-heme iron in its electronic structure and reactivity.

Studies of BLM were extended to elucidate the geometric and electronic structural changes of BLM/Fe^{II} upon interaction with its substrate, DNA, to gain further insight into the molecular mechanism of DNA cleavage and the effects of substrates which are themselves biological macromolecules. MCD spectra of BLM/Fe^{II} in complex with DNA (calf thymus or DNA oligonucleotides) showed a significant perturbation of the Fe^{II} active site compared to BLM/Fe^{II} in the absence of DNA as evidenced by the changes in the intensity ratio of the LF transitions of the 6C site (Fig. 13, top).[130] Analysis of the energies of the DNA-bound complexes showed a decrease in Δ^5E_g compared to BLM/Fe^{II} without DNA, consistent with a 6C Fe^{II} site that has a stronger axial ligand compared to BLM/Fe^{II}.

Parallel studies of the interactions of the Fe^{II}-BLM derivatives with DNA provided further insight into the structural perturbations which occur upon BLM binding to DNA.[130] In particular, while the MCD spectrum of *iso*-PEPLM/Fe^{II} in the absence of DNA is different from BLM/Fe^{II} (Fig. 10), binding to DNA resulted in a spectrum similar to that for BLM/Fe^{II} bound to DNA. This result is consistent with a structural model where the mannose carbamoyl provides an axial ligand to Fe^{II} (or the mannose carbamoyl may interact through significant second sphere effects), but binding to DNA removes the sugar group from ligation (Fig. 13, bottom). Therefore, the decrease in Δ^5E_g of BLM/Fe^{II} when bound to DNA is the result of the loss of the

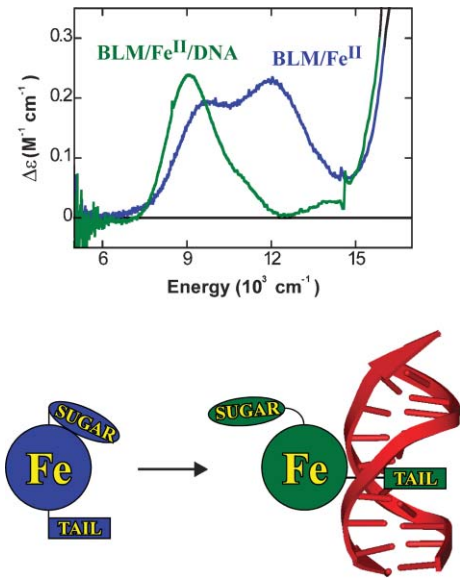

Fig. 13 MCD (top) and structural model (bottom) for BLM/Fe^{II} binding to DNA.

carbamoyl ligand and its replacement by solvent. This reflects a strong binding of the Fe^{II} site to DNA which orients the product of the reaction of BLM/Fe^{II} plus an electron with dioxygen (*i.e.* activated bleomycin) for reaction at the C′H bond of the sugar backbone of DNA.[96]

E. PKU-inducing mutants of PAH

While elucidation of the active site geometric and electronic structures of the mononuclear non-heme iron enzymes has provided insight into their proper functioning, insight can also be gained into the active site changes that lead to poor or no catalysis. It is the improper functioning of these enzymes which can lead to serious diseases in humans. In particular, dysfunction of phenylanine hydroxylase leads to the disease phenylketonuria (PKU) in which accumulation of toxic L-Phe metabolites leads to severe and irreversible mental retardation.[50,51] Two mutants of PAH, R158Q and E280K, induce PKU and have been shown to be only ~20% coupled to production of L–Tyr product. Product analyses show that both mutants oxidize pterin at a rate more than twice that of wild-type PAH (wt-PAH).[131] To obtain insight into the molecular mechanisms of this disease, these PKU-inducing mutants were investigated by MCD spectroscopy to probe the active site geometric and electronic structure perturbations arising from these mutations and their relation to reactivity.

MCD spectroscopy has shown that resting PAH is a purely 6C species which is converted to a 5C species only when both pterin and L-Phe are bound.[52,53] It is the 5C Fe^{II} site in the presence of both cofactor and substrate which activates dioxygen for the coupled reaction and product formation, in accordance with the general mechanistic strategy for oxygen activation (see Section IIIA-1). Comparison of the MCD spectra of wt-PAH, R158Q-PAH and E280K-PAH shows that both mutations result in resting Fe^{II} sites that are 6C species with two LF transitions at similar energies with similar Δ^5E_g excited-state splittings to wt-PAH (Fig. 14A).[131] In addition, from VTVH-MCD the $^5T_{2g}$ ground state parameters are the same within error for the three resting sites.

The quaternary complex of the R158Q mutant of PAH with Fe^{II}, pterin analog 5-deaza-6-MPH_4 and L-Phe bound exhibits an MCD spectrum similar to wt-PAH (Fig. 14B, red and blue), with the presence of a low energy (<5000 cm^{-1}) LF transition indicative of a 5C component. In contrast, the corresponding quaternary complex of the E280K mutant of PAH with Fe^{II}, pterin and L-Phe results in a different MCD spectrum from

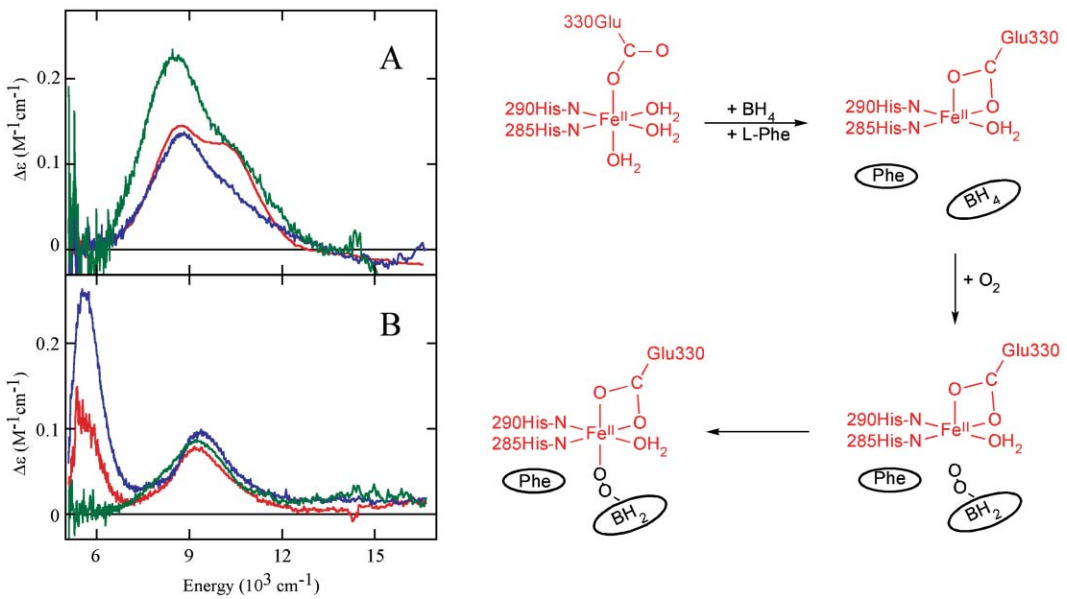

Fig. 14 MCD spectra of PKU-inducing mutants of PAH (left). (A) MCD of wt-PAH/Fe^{II} (red), R158Q-PAH/Fe^{II} (blue) and E280K-PAH/Fe^{II} (green) and (B) MCD of wt-PAH/Fe^{II}/5-deaza-6-MPH_4/L-Phe (red), R158Q-PAH/Fe^{II}/5-deaza-6-MPH_4/L-Phe (blue) and E280K-PAH/Fe^{II}/5-deaza-6-MPH_4/L-Phe (green). Scheme for dioxygen activation in PAH (right).

wt-PAH or R158Q-PAH, where the lower energy 5C band is completely absent in E280K-PAH (Fig. 14B, green). In fact, analysis of the LF transitions of the E280K-PAH/Fe^{II}/5-deaza-6-MPH_4/L-Phe shows that only two transitions are present at 9100 and 10800 cm^{-1}, indicative of a purely 6C Fe^{II} site in this mutant.

Combined with kinetic data, these MCD studies of the PKU-inducing mutants provide important insight into the molecular mechanism of PAH. While both mutants oxidize pterin at a rate more than twice wt-PAH, the MCD spectra of the two mutants bound to pterin and substrate show that R158Q-PAH is 5C while E280K-PAH is 6C. As the 6C site of the E280K mutant is coordinatively saturated, dioxygen would not directly react with the Fe^{II} site for activation. Thus, the fact that both mutants oxidize pterin more rapidly than wt-PAH despite their coordination differences supports a mechanism for oxygen activation in which dioxygen first reacts with the pterin cofactor to yield a peroxy-pterin species (Fig. 14, right). Subsequently, this peroxy-pterin intermediate would react with the Fe^{II} site to form an Fe–OO-pterin bridge. However, formation of this bridge would require an open coordination position on the Fe^{II} site and be dependent upon the pterin orientation relative to the Fe^{II} site. While pterin oxidation is observed for both mutants, the MCD data of the E280K-PAH mutant shows that no open coordination position would be available to form the Fe–OO-pterin bridge as the site is 6C, due to possible perturbations of either or both pterin and L-Phe binding. While this is not the case for the R158Q mutant which has a 5C Fe^{II} site, the observed uncoupling of the reaction likely reflects a change in the orientation of the pterin cofactor relative to the Fe^{II} site, preventing the formation of the Fe–OO-pterin bridge following pterin oxidation. For the bridged Fe–OO-pterin species in the wt enzyme, cleavage of the O–O bridge would generate an Fe^{IV}=O species which could electrophilically attack the L-Phe aromatic ring to yield the hydroxylated product, L-Tyr.

IV. Oxygen intermediates

The application of the Fe^{II} methodology to active sites of mononuclear non-heme iron enzymes has provided important insight into structure–function correlations in these systems as described in section III. Importantly, the activation of dioxygen by these non-heme iron enzymes in principle involves iron-oxygen intermediates that are the active oxidizing species for the reactions catalyzed. Depending upon the nature of the non-heme Fe^{II} active site and the number of reducing equivalents available from cofactors and substrates for oxygen activation, two general types of iron-oxygen intermediates can be considered: Fe^{III}-peroxide and Fe^{IV}=O species. Direct insight into the nature of the iron-oxygen intermediates in the reaction pathways of these enzymes has historically been limited by the lack of available trapped intermediates. However, recent studies of trapped intermediates in the reactions of mononuclear non-heme iron enzymes and correlation to studies of model complexes combined with DFT calculations have provided insight into the nature of these intermediates and the reaction pathways of the enzymes.

A. Peroxide level intermediates

Since the Rieske cofactor present in the Rieske dioxygenases is a one electron donor, the reaction of the Fe^{II} enzyme likely leads to an Fe^{III}-peroxide intermediate generated by the two electron reduction of dioxygen.[90–93] A recent crystallographic study of one member of this class of enzymes, naphthalene dioxygenase (NDO) in the presence of the alternative substrate indole, has identified a side-on bound (η^2) dioxygen-iron species (Fig. 15A).[94] The dioxygen molecule is well oriented for attack by both oxygen atoms on the double bond of the aromatic substrate. While this structure supports the possibility of a side-on bound Fe^{III}-peroxide intermediate as the iron-oxygen intermediate in NDO, further studies are required to elucidate its electronic structure and evaluate its reactivity.

Previous spectroscopic and theoretical studies of a side-on bound (η^2) dioxygen model system, the EDTA/Fe^{III}/peroxide complex, provided insight into its electronic structure and possible contributions to reactivity in mononuclear non-heme iron enzymes.[132] Using a methodology similar to that summarized in section II but developed for Fe^{III} sites in ref. 1, these studies showed that the Fe^{III}–peroxide interaction is dominated by a strong covalent σ-bond between the π_σ* and Fe(d_{xy}) orbitals (Fig. 15B) with only weak interactions of π- and δ-symmetry. Importantly, as no backbonding between Fe^{III} and the peroxide σ*-orbital was observed, the O–O bond was not activated beyond the peroxide level consistent with its low reactivity towards organic substrates.[133] However, there is not much peroxide character in the LUMO and the electron density is mostly in the peroxide bonding orbital. Thus, the η^2-peroxide is nucleophilic and activated for protonation. As decribed below, the effect of protonation would be to lower the energy of the O_2^{2-} σ^* orbital and activate it for electrophilic attack on a substrate, potentially an aromatic ring.

Activated bleomycin (ABLM) was the first extensively studied trapped intermediate in a mononuclear non-heme iron system and shown to be kinetically competent to cleave DNA by H-atom abstraction.[134] Formed upon reaction of BLM/Fe^{II} with dioxygen and an exogenous electron, ABLM has been determined to be a low spin Fe^{III}–OOH complex.[102–106] The electronic and geometric structures of ABLM have been elucidated from a combination of spectroscopic studies (Abs,

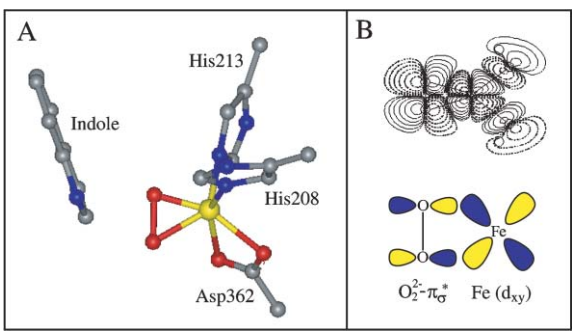

Fig. 15 (A) Crystal structure of NDO in the presence of indole with a side-on bound (η^2) dioxygen-iron species (from PDB file 107N), (B) contour plot (top) and schematic representation (bottom) of the strong σ-bond between the Fe(d_{xy}) and peroxide π_σ* orbitals in the EDTA/Fe^{III}/peroxide complex.

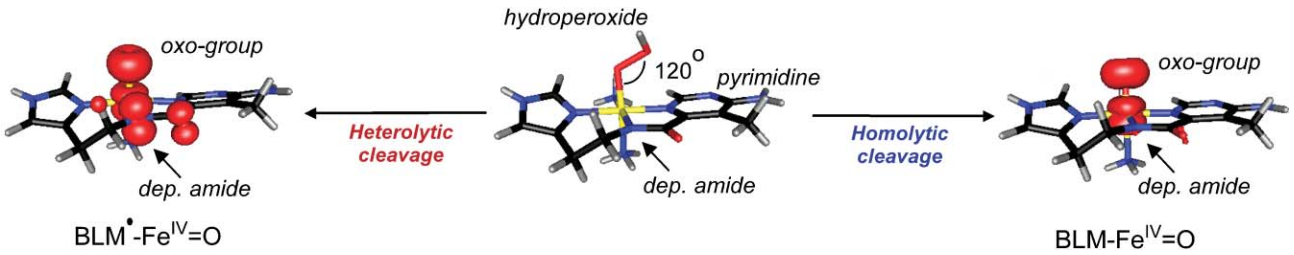

Fig. 16 Possible reaction mechanisms for H-atom abstraction of DNA by ABLM: homolytic and heterolytic O–O bond cleavage.

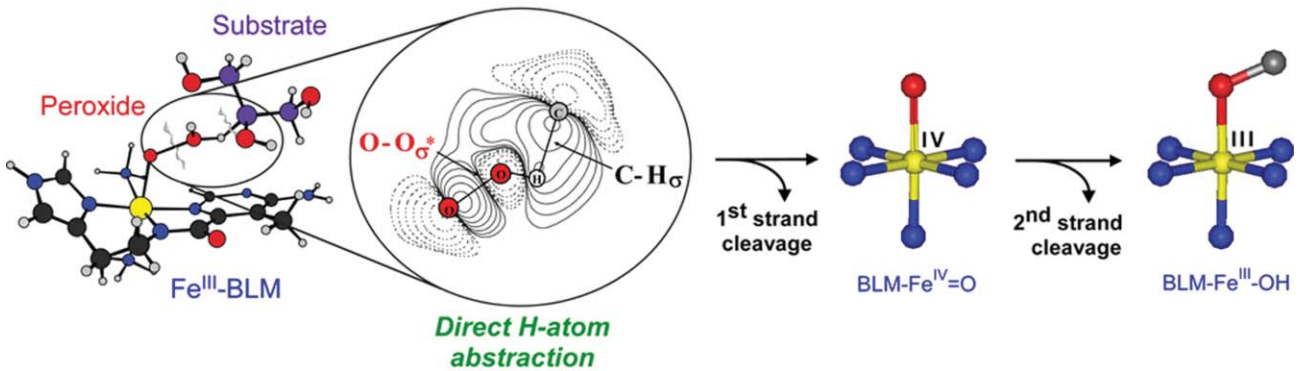

Fig. 17 Single-strand DNA cleavage by direct H-atom abstraction by ABLM and second H-atom abstraction by the resulting BLM-Fe^{IV}=O to yield double-strand cleavage.

CD, MCD, resonance Raman, EPR, XAS) and electronic structure calculations (DFT, Hartree–Fock, semiempirical).[135] The resulting geometry optimized structure of ABLM (Fig. 16, center) consists of a hydroperoxide bound with an Fe–O–O angle of 120°, bisecting the deprotonated amide and pyrimidine nitrogens of the equatorial glycopeptide ligands.

The experimentally correlated geometric-optimized structure of ABLM was utilized to evaluate possible mechanisms for the H-atom abstraction reaction of ABLM toward DNA: (1) heterolytic cleavage of the O–O bond to generate a formally Fe^{V}=O species (Fig. 16, left), (2) homolytic cleavage yielding an Fe^{IV}=O intermediate (Fig. 16, right) or (3) direct H-atom abstraction by the hydroperoxy complex (Fig. 17).[135] Calculation of the heterolytic reaction was found to produce an Fe^{IV}=O species combined with oxidation of the deprotonated amide of the ligand, analogous to compound I in heme systems ($[Fe^{IV}=O(Por^{\cdot})]^{+}$) (Fig. 16, left). Heterolytic cleavage of the O–O bond in ABLM was calculated to be $\sim$175 kcal mol^{-1} higher in energy than the corresponding reaction for a Fe-porphyrin-thiolate model of cytochrome P450.[136] One reason for this difference is the ease of oxidation of the heme *vs.* the non-heme BLM ligand. Direct evaluation of the relative energies of oxidation of the two ligand systems was determined from the energies of the LMCT transitions assigned by MCD, where the deprotonated amide-to-Fe^{III}BLM CT transition was found to be almost 2.5 eV higher in energy than the porphyrin-to-Fe^{III} LMCT transition.[135] An additional contribution to the different energies of heterolysis is the higher negative charge in the heme system which stabilizes the oxidized heme site relative to the non-heme site. Since the ligands of the non-heme iron enzymes are even more difficult to oxidize than the BLM ligand, heterolysis is likely to be energetically unfavorable.

Another possible mechanism for the reaction of ABLM is homolytic cleavage of the O–O bond yielding an Fe^{IV}=O intermediate and a free $^{\cdot}$OH radical (Fig. 16, right). O–O homolysis has been found to occur for several low-spin Fe^{III}-hydroperoxy complexes. The spectroscopic properties and electronic structures of ABLM compared to these model complexes ($[Fe(N4Py)(OOH)]^{2+}$ (where N4Py = *N*,*N*-bis(2-pyridylmethyl)-*N*-bis(2-pyridyl)methylamine) and [Fe(TPA)-(solv)$(OOH)]^{x+}$ (where TPA = tris(2-pyridylmethyl)amine) and solv is likely water or hydroxide)), while generally very similar, did exhibit an interesting difference.[137] This is the rotation of the hole in the t_{2g} shell by the π-donating deprotonated amide in ABLM, which reduces the π-donor bond of the HO_2^{-} to Fe^{III} as evidenced by the lack of the corresponding CT transition. However, DFT calculations indicate that this difference in the electronic structure of ABLM is minimized along the reaction coordinate and does not play a significant role in homolysis. Therefore, ABLM should be thermodynamically and kinetically competent to undergo O–O homolysis.

While DFT studies of ABLM suggest that O–O homolysis is energetically possible, kinetic studies of ABLM have suggested a different reactivity based upon the high kinetic isotope effect (KIE) of the reaction of ABLM with DNA ($k_H/k_D \approx 2$–7).[138] This is in contrast to the small KIEs that have been observed for free $^{\cdot}$OH radicals[139,140] and the radical based reaction of CoBLM with DNA.[138,141] Since the homolytic cleavage mechanism involves free $^{\cdot}$OH radicals, this observation argues for direct H-atom abstraction from the sugar moiety of DNA by the low spin Fe^{III}–OOH complex to yield Fe^{IV}BLM=O, a DNA radical and water.[135] While direct H-atom abstraction is closely related to O–O homolysis, it differs in that homolysis of

the O–O bond is coupled to cleavage of a C–H bond and formation of a stronger O–H bond along the reaction coordinate, resulting in a lower overall reaction energy. Thus, binding to DNA appears to direct the reactivity of ABLM towards direct H-atom abstraction.

As suggested above for the high-spin η^2-peroxide-Fe^{III} complex, calculation of the low-spin Fe^{III} hydroperoxide complex of ABLM showed that protonation of the peroxide greatly lowers the energy of its σ* orbital. This activates the hydroperoxide for electrophilic attack on the C–H σ bond of the substrate (Fig. 17, expanded section) and results in a shift in electron density onto the σ* orbital from the H–C bond, weakening both bonds and promoting H-atom transfer to form water.[135] In addition, the high affinity of ABLM for DNA and the resulting orientation of the σ* orbital of the hydroperoxide for H-atom abstraction (from the NMR structure of the CoBLM-DNA complex[142]) also contributes to the direct H-atom abstraction. The H-atom abstraction will produce an Fe^{IV}=O intermediate (Fig. 17, middle) capable of a second H-atom abstraction from DNA for double-stranded DNA cleavage. The anticancer activity of this drug relates to its double strand cleavage which is not easily repaired.[95,97]

B. Fe^{IV}=O intermediates

In mononuclear non-heme iron enzymes other than the Rieske dioxygenases and the drug BLM, cofactors or substrates capable of donating two electrons to the reduction of dioxygen are present and these enzymes have often been proposed to utilize high-valent Fe^{IV}=O intermediates as the active oxidizing species. Recently, the first direct characterization of an Fe^{IV}=O intermediate in a mononuclear non-heme iron enzyme has been achieved in the α-KG-dependent dioxygenase TauD, as supported by Mössbauer (δ = 0.31 mm s^{-1}, ΔE_Q = 0.88 mm s^{-1}),[78] resonance Raman ($\upsilon_{Fe=O}$ = 821 cm^{-1})[79] and EXAFS ($r_{Fe=O}$ = 1.62 Å)[80] studies. This species has a high-spin S = 2 ground state and reacts with substrate by H-atom abstraction, with subsequent rebound hydroxylation by the resulting Fe^{III}–OH^- species proposed to yield hydroxylated product.

Several Fe^{IV}=O complexes have been synthesized and characterized as models of the high-valent intermediates in these enzymes. All the models to date are low-spin S = 1 complexes with a 6C axially-distorted non-heme ligand set.[143–146] Utilizing a methodology developed for Fe^{IV} sites in ref. 147 involving a combination of VTVH-MCD and experimentally calibrated DFT calculations, the electronic structure description of one of these complexes, $[Fe(O)(TMC)(NCCH_3)]^{2+}$, has been determined and provides a basis for understanding the nature of the Fe^{IV}=O intermediates in non-heme iron enzymes.[147] Five ligand-field transitions are observed in the absorption and MCD spectra of $[Fe(O)(TMC)(NCCH_3)]^{2+}$ (Fig. 18A), consistent with group theory for a d^4 S = 1 system with C_{4v} symmetry. These can be assigned based on their polarizations determined from the temperature dependence of the MCD spectra. While determination of the polarizations of transitions typically requires single crystal spectroscopy, VTVH-MCD allows elucidation of the transition polarizations for a

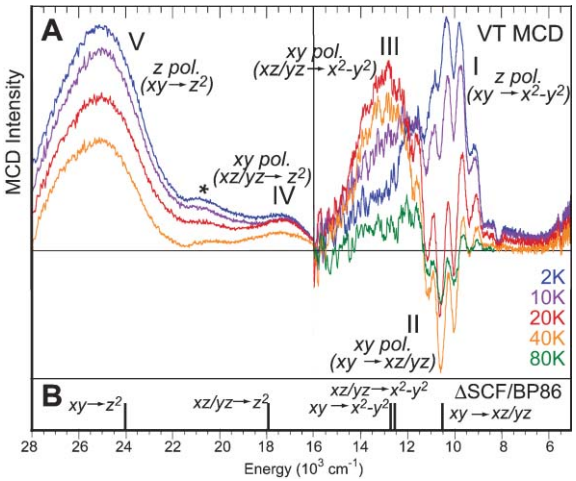

Fig. 18 Spectroscopic and computational studies of the $[Fe(O)(TMC)(NCCH_3)]^{2+}$ model complex: (A) LT MCD and (B) calculated transition energies. Adapted from ref. 147.

randomly oriented set of molecules. Assignment is assisted by analysis of the observed vibronic structure. Band I is assigned to the $d_{xy} \rightarrow d_{x2-y2}$ transitions and its energy position reflects the equatorial ligand strength (Fig. 19). Band II and Band III, both *xy*-polarized, are assigned to the $d_{xy} \rightarrow d_{xz/yz}$ and $d_{xz/yz} \rightarrow d_{x2-y2}$ transitions, respectively. The $d_{xy} \rightarrow d_{xz/yz}$ transition reflects the oxo–iron π-bond strength and has a vibronic progression associated with it due to weakening of the Fe–O bond due to excitation of an electron from the non-bonding d_{xy} orbital to the Fe–O π-antibonding $d_{xz/yz}$ orbitals. Band IV is assigned to the *xy*-polarized $d_{xz/yz} \rightarrow d_{z^2}$ transition, where the difference in energy between Bands III and IV (4500 cm^{-1}) gives the splitting of the e_g set of d-orbitals due to the σ* ineraction of the oxo-ligand. Band V is assigned to the $d_{xy} \rightarrow d_{z^2}$ transition and reflects the strength of the iron-oxo σ-bond.

The geometry optimized structure of the $[Fe(O)(TMC)(NCCH_3)]^{2+}$ complex was calculated using DFT and found to agree well with the reported crystal

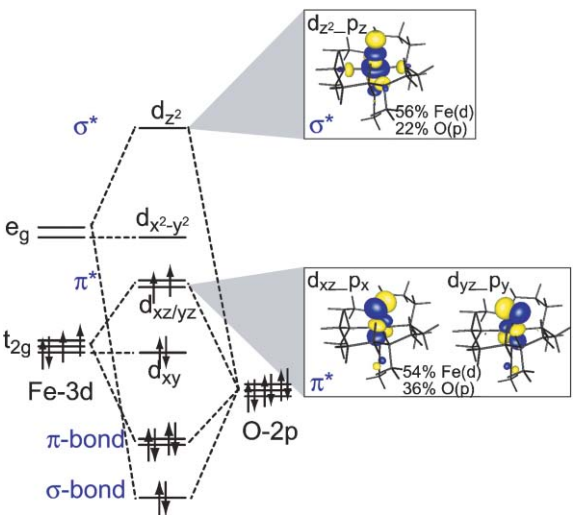

Fig. 19 Fe^{IV}=O bonding scheme and contour plots of the orbitals involved in Fe–O σ- and π-bonding.

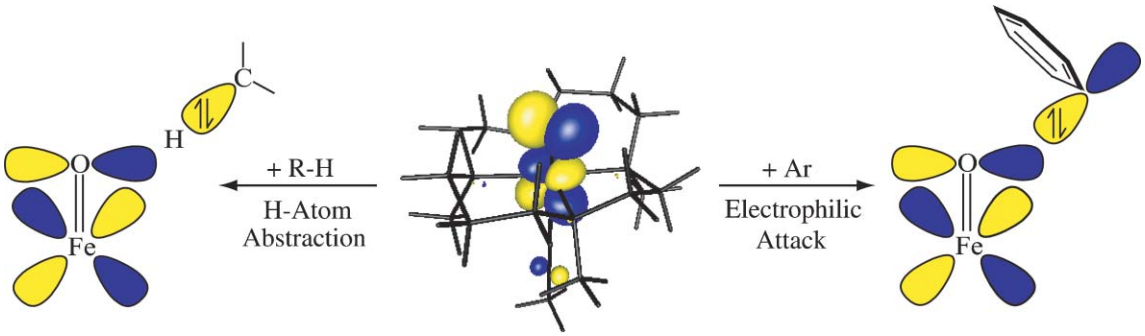

Fig. 20 Fe^{IV}=O reactivity for H-atom abstraction and electrophilic attack in terms of FMO theory.

structure.[147] In addition, the calculated transition energies correlated well with those determined by spectroscopy (Fig. 18B). Therefore, the calculations were extended to gain further insight into the bonding of an $S = 1$ Fe^{IV}=O as generated by the first H-atom abstraction by ABLM and also associated with H-atom abstraction in double strand DNA cleavage and $S = 2$ Fe^{IV}=O species that would be related to iron-oxygen intermediates in non-heme iron enzymes. The iron–oxo bonding and activation were found to be very similar in both the $S = 1$ and $S = 2$ spin states. This is due to the fact that the $S = 2$ state involves excitation of one electron from the d_{xy} to the d_{x2-y2} orbital (combined with a spin flip in Fig. 19), where the d_{xy} and d_{x2-y2} orbitals are perpendicular to the Fe–O bond and do not interact with the oxo ligand. However, while the calculated bond lengths, vibrational frequencies and orbital coefficients for the $S = 2$ Fe^{IV}=O are comparable to that for the $S = 1$ complex, the spectroscopies should be different as an $S = 2$ Fe^{IV}=O, a d^4 complex with C_{4v} symmetry, would exhibit only one allowed d → d transition.

For both complexes, the calculated energy splitting of the d_{xy} and $d_{xz/yz}$ orbitals due to π-bonding, the σ-bond splitting of the e_g set and the large mixing of Fe(d) and O(p) orbitals support the presence of an Fe–O unit with one strong σ- and two strong ½ π-bonds (Fig. 19). In terms of FMO theory, the strong Fe-oxo π-donor bond results in significant oxo character in the low-lying, unoccupied Fe d_{xz}/d_{yz} orbitals (Fig. 20). This activates the oxygen atom for H-atom abstraction and electrophilic attack on π-rings.

V. Conclusion

The application of an Fe^{II} methodology utilizing CD and MCD spectroscopies has been a powerful tool for obtaining molecular level insight into the active site geometric and electronic structures of mononuclear non-heme iron enzymes which activate dioxygen for a wide variety of biological reactions. MCD combined with DFT calculations has also been instrumental in determining the electronic structure of peroxo and oxo intermediates and identifying the fundamental bonding interactions associated with reactivity. As described in this review, these studies have defined important structure–function correlations in these enzymes and provided key insights into oxygen activation, reactivities and many other contributions to catalysis.

Acknowledgements

E. I. S. thanks the following collaborators for their outstanding contributions to the research on oxygen activating mononuclear non-heme iron enzymes: Jeffrey T. Bolin (Purdue University) on DHBD, John P. Caradonna (Boston University) on PAH, Walter R. Ellis, Jr. (University of Utah) on PDO, Lindsay D. Eltis (University of British Columbia) on DHBD, Britt Hedman and Keith O. Hodgson (Stanford University and Stanford Synchrotron Radiation Laboratory) on XAS, Theodore R. Holman (University of California, Santa Cruz) on sLO, the late Nobumasa Kitajima (Tokyo Institute of Technology) on Fe^{II} coordination complexes, John D. Lipscomb (University of Minnesota) on ACCO and intra- and extradiol dioxygenases, Pradip K. Mascharak (University of California, Santa Cruz) on BLM analogs, Sidney M. Hecht (University of Virginia) on BLM derivatives, Graham R. Moran (University of Wisonsin-Milwaukee) on HPPD, Lawrence Que, Jr. (University of Minnesota) on iron-oxygen models and ACCO, Jonathan B. Spencer (University of Cambridge) on HmaS, and Craig A. Townsend (The Johns Hopkins University) on CS2. E. I. S. also thanks all his current and former students for their outstanding contributions to this research. This work was supported by NIH (GM-40392) and an NSF graduate fellowship (M. L. N.).

References

1 E. I. Solomon, T. C. Brunold, M. I. Davis, J. N. Kemsley, S.-K. Lee, N. Lehnert, F. Neese, A. J. Skulan, Y.-S. Yang and J. Zhou, *Chem. Rev.*, 2000, 235–349.
2 J. N. Siedow, *Annu. Rev. Plant Physiol. Plant Mol. Biol.*, 1991, **42**, 145–188.
3 A. W. Ford-Hutchinson, M. Gresser and R. N. Young, *Annu. Rev. Biochem.*, 1994, **63**, 383–417.
4 S. Yamamoto, *Biochim. Biophys. Acta*, 1992, **1128**, 117–131.
5 G. A. Veldink and J. F. G. Vliegenhart, *Adv. Inorg. Biochem.*, 1984, **6**, 139–161.
6 B. Samuelsson, S. E. Dahlen, J. A. Lindgren, C. A. Rouzer and C. N. Serhan, *Science*, 1987, **237**, 1171–1176.
7 E. Sigal, *Am. J. Physiol.*, 1991, **260**, L13–L28.
8 K. V. Honn, D. G. Tang, X. Gao, I. A. Butovich, B. Liu, J. Timar and W. Hagmann, *Cancer Metastasis Rev.*, 1994, **13**, 365–396.
9 V. E. Steele, C. A. Holmes, E. T. Hawk, L. Kopelovich, R. A. Lubet, J. A. Crowell, C. C. Sigman and G. J. Kelloff, *Cancer Epidemiol. Biomarkers Prev.*, 1999, **8**, 467–483.
10 J. C. Boyington, B. J. Gaffney and L. M. Amzel, *Science*, 1993, **260**, 1482–1486.

11 W. Minor, J. Steczko, B. Stec, Z. Otwinowski, J. T. Bolin, R. Walter and B. Axelrod, *Biochemistry*, 1996, **35**, 10687–10701.
12 D. R. Tomchick, P. Phan, M. Cymborowski, W. Minor and T. R. Holman, *Biochemistry*, 2001, **40**, 7509–7517.
13 M. A. Pavlosky, Y. Zhang, T. E. Westre, Q.-F. Gan, E. G. Pavel, C. Campochiaro, B. Hedman, K. O. Hodgson and E. I. Solomon, *J. Am. Chem. Soc.*, 1995, **117**, 4316–4327.
14 R. C. Scarrow, M. G. Trimitsis, C. P. Buck, G. N. Grove, R. A. Cowling and M. J. Nelson, *Biochemistry*, 1994, **33**, 15023–15035.
15 Y. Zhang, M. S. Gebhard and E. I. Solomon, *J. Am. Chem. Soc.*, 1991, **113**, 5162–5175.
16 E. I. Solomon, J. Zhou, F. Neese and E. G. Pavel, *Chem. Biol.*, 1997, **4**, 795–808.
17 H. W. Gardner, *Biochim. Biophys. Acta*, 1989, **1001**, 274–281.
18 M. H. Glickman and J. P. Klinman, *Biochemistry*, 1996, **35**, 12882–12892.
19 N. Lehnert and E. I. Solomon, *J. Biol. Inorg. Chem.*, 2003, **8**, 294–305.
20 T. E. Elgren, A. M. Orville, K. A. Kelly, J. D. Lipscomb, D. H. Ohlendorf and L. Que, *Biochemistry*, 1997, **36**, 11504–11513.
21 R. W. Frazee, A. M. Orville, K. B. Dolbeare, H. Yu, D. H. Ohlendorf and J. D. Lipscomb, *Biochemistry*, 1998, **37**, 2131–2144.
22 A. M. Orville, J. D. Lipscomb and D. H. Ohlendorf, *Biochemistry*, 1997, **36**, 10052–10066.
23 A. M. Orville, N. Elango, J. D. Lipscomb and D. H. Ohlendorf, *Biochemistry*, 1997, **36**, 10039–10051.
24 D. H. Ohlendorf, A. M. Orville and J. D. Lipscomb, *J. Mol. Biol.*, 1994, **244**, 586–608.
25 M. W. Vetting, D. A. D'Argenio, L. N. Ornston and D. H. Ohlendorf, *Biochemistry*, 2000, **39**, 7943–7955.
26 H. Fujisawa and O. Hayaishi, *J. Biol. Chem.*, 1968, **243**, 2673–2681.
27 L. Que, Jr. and R. H. H. II, *J. Am. Chem. Soc.*, 1979, **101**, 2219–2221.
28 C. Bull, D. P. Ballou and I. Salmeen, *Biochem. Biophys. Res. Commun.*, 1979, **87**, 836–841.
29 M. I. Davis, A. M. Orville, F. Neese, J. M. Zaleski, J. D. Lipscomb and E. I. Solomon, *J. Am. Chem. Soc.*, 2002, **124**, 602–614.
30 J. W. Whittaker and J. D. Lipscomb, *J. Biol. Chem.*, 1984, **259**, 4487–4495.
31 A. M. Orville and J. D. Lipscomb, *J. Biol. Chem.*, 1989, **264**, 8791–8801.
32 A. E. True, A. M. Orville, L. L. Pearce, J. D. Lipscomb and L. Que, *Biochemistry*, 1990, **29**, 10847–10854.
33 J. D. Lipscomb and A. M. Orville, in *Metal Ions in Biological Systems*, ed. H. Sigel and A. Sigel, Marcel Dekker, New York, 1992, pp. 243–299.
34 L. Que, Jr., R. C. Kolanczyk and L. S. White, *J. Am. Chem. Soc.*, 1987, **109**, 5373–5380.
35 D. D. Cox and L. Que, Jr., *J. Am. Chem. Soc.*, 1988, **110**, 8085–8092.
36 G. Schenk, M. Y. M. Pau and E. I. Solomon, *J. Am. Chem. Soc.*, 2004, **126**, 505–515.
37 S. Han, L. D. Eltis, K. N. Timmis, S. W. Muchmore and J. T. Bolin, *Science*, 1995, **270**, 976–980.
38 Y. Uragami, T. Senda, K. Sugimoto, N. Sato, V. Nagarajan, E. Masai, M. Fukuda and Y. Mitsui, *J. Inorg. Biochem.*, 2001, **83**, 269–279.
39 S. D. Dai, F. H. Vaillancourt, H. Maaroufi, H. M. Drouin, D. B. Neau, V. Snieckus, J. T. Bolin and L. D. Eltis, *Nat. Struct. Biol.*, 2002, **9**, 934–939.
40 M. I. Davis, E. C. Wasinger, A. Decker, M. Y. M. Pau, F. H. Vaillancourt, J. T. Bolin, L. D. Eltis, B. Hedman, K. O. Hodgson and E. I. Solomon, *J. Am. Chem. Soc.*, 2003, **125**, 11214–11227.
41 P. A. Mabrouk, A. M. Orville, J. D. Lipscomb and E. I. Solomon, *J. Am. Chem. Soc.*, 1991, **113**, 4053–4061.
42 F. H. Vaillancourt, C. J. Barbosa, T. G. Spiro, J. T. Bolin, M. W. Blades, R. F. B. Turner and L. D. Eltis, *J. Am. Chem. Soc.*, 2002, **124**, 2485–2496.
43 E. L. Hegg and L. Que, Jr., *Eur. J. Biochem.*, 1997, **250**, 625–629.
44 L. Que, *Nat. Struct. Biol.*, 2000, **7**, 182–184.
45 K. D. Koehntop, J. P. Emerson and L. Que, *J. Biol. Inorg. Chem.*, 2005, **10**, 87–93.
46 G. P. Titus, H. A. Mueller, J. Burgner, S. R. D. Córdoba, M. A. Peñalva and D. E. Timm, *Nat. Struct. Biol.*, 2000, **7**, 542–546.
47 P. L. Roach, I. J. Clifton, V. Fülöp, K. Harlos, G. J. Barton, J. Hajdu, I. Andersson, C. J. Schofield and J. E. Baldwin, *Nature*, 1995, **375**, 700–704.
48 P. L. Roach, I. J. Clifton, C. M. H. Hensgens, N. Shibata, C. J. Schofield, J. Hajdu and J. E. Baldwin, *Nature*, 1997, **387**, 827–830.
49 T. J. Kappock and J. P. Caradonna, *Chem. Rev.*, 1996, **96**, 2659–2756.
50 M. Weinstein, R. C. Eisensmith, V. Abadie, S. Avigad, S. Lyonnet, G. Schwartz, A. Munnich, S. L. C. Woo and Y. Shiloh, *Hum. Genet.*, 1993, **90**, 645–649.
51 P. J. Waters, M. A. Parniak, B. R. Akerman, A. O. Jones and C. R. Scriver, *J. Inher. Metab. Dis.*, 1999, **22**, 208–212.
52 K. E. Loeb, T. E. Westre, T. J. Kappock, N. Mitic, E. Glasfeld, J. P. Caradonna, B. Hedman, K. O. Hodgson and E. I. Solomon, *J. Am. Chem. Soc.*, 1997, **119**, 1901–1915.
53 J. N. Kemsley, N. Mitic, K. Loeb Zaleski, J. P. Caradonna and E. I. Solomon, *J. Am. Chem. Soc.*, 1999, **121**, 1528–1536.
54 E. C. Wasinger, N. Mitic, B. Hedman, J. Caradonna, E. I. Solomon and K. O. Hodgson, *Biochemistry*, 2002, **41**, 6211–6217.
55 T. J. Kappock, P. C. Harkins, S. Friedenberg and J. P. Caradonna, *J. Biol. Chem.*, 1995, **270**, 30532–30544.
56 A. Tourian, *Biochim. Biophys. Acta*, 1971, **242**, 345–354.
57 T. Xia, D. W. Gray and R. Shiman, *J. Biol. Chem.*, 1994, **269**, 24657–24665.
58 T. A. Dix and S. J. Benkovic, *Acc. Chem. Res.*, 1988, **21**, 101–107.
59 G. Guroff, J. W. Daly, D. M. Jerina, J. Renson, B. Witkop and S. Udenfriend, *Science*, 1967, **157**, 1524–1530.
60 R. P. Hausinger, *Crit. Rev. Biochem. Mol. Biol.*, 2004, **39**, 21–68.
61 K. I. Kivirikko and R. Myllylä, in *The Enzymology of Post-Translational Modification of Proteins*, ed. R. B. Freedman and H. C. Hawkins, Academic, London, 1980, pp. 53–104.
62 M. J. Ryle, R. Padmakumar and R. P. Hausinger, *Biochemistry*, 1999, **38**, 15278–15286.
63 J. E. Baldwin, K. D. Merritt, C. J. Schofield, S. W. Elson and K. H. Baggaley, *J. Chem. Soc., Chem. Commun.*, 1993, 1301–1302.
64 S. W. Elson, K. H. Baggaley, J. Gillett, S. Holland, N. H. Nicholson, J. T. Sime and S. R. Woroniecki, *J. Chem. Soc., Chem. Commun.*, 1987, 1736–1740.
65 W. J. Krol, A. Basak, S. P. Salowe and C. A. Townsend, *J. Am. Chem. Soc.*, 1989, **111**, 7625–7627.
66 J. E. Baldwin and E. Abraham, *Nat. Prod. Rep.*, 1988, **5**, 129–145.
67 P. O. Falnes, *Nucleic Acids Res.*, 2004, **32**, 6260–6267.
68 P. O. Falnes, R. F. Johansen and E. Seeberg, *Nature*, 2002, **419**, 178–182.
69 S. C. Trewick, T. F. Henshaw, R. P. Hausinger, T. Lindahl and B. Sedgwick, *Nature*, 2002, **419**, 174–178.
70 C. J. Schofield and P. J. Ratcliffe, *Nat. Rev. Mol. Cell Biol.*, 2004, **5**, 343–354.
71 E. G. Pavel, J. Zhou, R. W. Busby, M. Gunsior, C. A. Townsend and E. I. Solomon, *J. Am. Chem. Soc.*, 1998, **120**, 743–753.
72 J. Zhou, M. Gunsior, B. O. Bachmann, C. A. Townsend and E. I. Solomon, *J. Am. Chem. Soc.*, 1998, **120**, 13539–13540.
73 J. Zhou, W. L. Kelly, B. O. Bachman, M. Gunsior, C. A. Townsend and E. I. Solomon, *J. Am. Chem. Soc.*, 2001, **123**, 7388–7398.
74 K. Valegard, A. C. T. Vanscheltinga, M. D. Lloyd, T. Hara, S. Ramaswamy, A. Perrakis, A. Thompson, H. J. Lee, J. E. Baldwin, C. J. Schofield, J. Hajdu and I. Andersson, *Nature*, 1998, **394**, 805–809.
75 Z. H. Zhang, J. S. Ren, D. K. Stammers, J. E. Baldwin, K. Harlos and C. J. Schofield, *Nat. Struct. Biol.*, 2000, **7**, 127–133.
76 J. M. Elkins, M. J. Ryle, I. J. Clifton, J. C. D. Hotopp, J. S. Lloyd, N. I. Burzlaff, J. E. Baldwin, R. P. Hausinger and P. L. Roach, *Biochemistry*, 2002, **41**, 5185–5192.
77 J. M. Elkins, K. S. Hewitson, L. A. McNeill, J. F. Seibel, I. Schlemminger, C. W. Pugh, P. J. Ratcliffe and C. J. Schofield, *J. Biol. Chem.*, 2003, **278**, 1802–1806.

78 J. C. Price, E. W. Barr, B. Tirupati, J. M. Bollinger and C. Krebs, *Biochemistry*, 2003, **42**, 7497–7508.
79 D. A. Proshlyakov, T. F. Henshaw, G. R. Monterosso, M. J. Ryle and R. P. Hausinger, *J. Am. Chem. Soc.*, 2004, **126**, 1022–1023.
80 P. J. Riggs-Gelasco, J. C. Price, R. B. Guyer, J. H. Brehm, E. W. Barr, J. M. Bollinger and C. Krebs, *J. Am. Chem. Soc.*, 2004, **126**, 8108–8109.
81 K. Johnson-Winters, V. M. Purpero, M. Kavana, T. Nelson and G. R. Moran, *Biochemistry*, 2003, **42**, 2072–2080.
82 O. W. Choroba, D. H. Williams and J. B. Spencer, *J. Am. Chem. Soc.*, 2000, **122**, 5389–5390.
83 J. E. Baldwin and M. Bradley, *Chem. Rev.*, 1990, **90**, 1079–1088.
84 P. John, *Physiol. Plant.*, 1997, **100**, 583–592.
85 A. G. Prescott, *J. Exp. Bot.*, 1993, **44**, 849–861.
86 I. Bertini, M. A. Cermonini, S. Ferretti, I. Lozzi, C. Luchinat and M. S. Viezzoli, *Coord. Chem. Rev.*, 1996, **151**, 145–160.
87 E. G. Pavel, L. J. Martins, W. R. Ellis, Jr. and E. I. Solomon, *Chem. Biol.*, 1994, **1**, 173–183.
88 G. T. Gassner, D. P. Ballou, G. A. Landrum and J. W. Whittaker, *Biochemistry*, 1993, **32**, 4820–4825.
89 B. Kauppi, K. Lee, E. Carredano, R. E. Parales, D. T. Gibson, H. Eklund and S. Ramaswamy, *Structure*, 1998, **6**, 571–586.
90 F. H. Bernhardt and H. H. Ruf, *Biochem. Soc. Trans.*, 1975, **3**, 878–881.
91 F. H. Bernhardt and H. Kuthan, *Eur. J. Biochem.*, 1981, **120**, 547–555.
92 P. Wende, F. H. Bernhardt and K. Pfleger, *Eur. J. Biochem.*, 1989, **181**, 189–198.
93 K. Lee, *J. Bacteriol.*, 1999, **181**, 2719–2725.
94 A. Karlsson, J. V. Parales, R. E. Parales, D. T. Gibson, H. Eklund and S. Ramaswamy, *Science*, 2003, **299**, 1039–1042.
95 J. Stubbe and J. W. Kozarich, *Chem. Rev.*, 1987, **87**, 1107–1136.
96 J. Stubbe, J. W. Kozarich, W. Wu and D. E. Vanderwall, *Acc. Chem. Res.*, 1996, **29**, 322–330.
97 R. M. Burger, *Chem. Rev.*, 1998, **98**, 1153–1169.
98 C. A. Claussen and E. C. Long, *Chem. Rev.*, 1999, **99**, 2797–2816.
99 J. Y. Chen and J. Stubbe, *Nat. Rev. Cancer*, 2005, **5**, 102–112.
100 K. E. Loeb, J. M. Zaleski, T. E. Westre, R. J. Guajardo, P. K. Mascharak, B. Hedman, K. O. Hodgson and E. I. Solomon, *J. Am. Chem. Soc.*, 1995, **117**, 4545–4561.
101 K. E. Loeb, J. M. Zaleski, C. D. Hess, S. M. Hecht and E. I. Solomon, *J. Am. Chem. Soc.*, 1998, **120**, 1249–1259.
102 R. M. Burger, J. Peisach and S. B. Horwitz, *J. Biol. Chem.*, 1981, **256**, 11636–11644.
103 J. W. Sam, X.-J. Tang and J. Peisach, *J. Am. Chem. Soc.*, 1994, **116**, 3250–5256.
104 R. M. Burger, G. Tian and K. Drlica, *J. Am. Chem. Soc.*, 1995, **117**, 1167–1168.
105 A. Veselov, H. Sun, A. Sienkiewicz, H. Taylor, R. M. Burger and C. P. Scholes, *J. Am. Chem. Soc.*, 1995, **117**, 7508–7512.
106 T. E. Westre, K. E. Loeb, J. M. Zaleski, B. Hedman, K. O. Hodgson and E. I. Solomon, *J. Am. Chem. Soc.*, 1995, **117**, 1309–1313.
107 J. W. Whittaker and E. I. Solomon, *J. Am. Chem. Soc.*, 1988, **110**, 5329–5339.
108 Y. Zhang, M. S. Gebhard and E. I. Solomon, *J. Am. Chem. Soc.*, 1991, **113**, 5162–5175.
109 E. I. Solomon, E. G. Pavel, K. E. Loeb and C. Campochiaro, *Coord. Chem. Rev.*, 1995, **144**, 369–460.
110 E. G. Pavel, N. Kitajima and E. I. Solomon, *J. Am. Chem. Soc.*, 1998, **120**, 3949–3962.
111 E. I. Solomon, E. G. Pavel, K. E. Loeb and C. Campochiaro, *Coord. Chem. Rev.*, 1995, **144**, 369–460.
112 C. Campochiaro, E. G. Pavel and E. I. Solomon, *Inorg. Chem.*, 1995, **34**, 4669–4675.
113 M. L. Neidig, M. Kavana, G. R. Moran and E. I. Solomon, *J. Am. Chem. Soc.*, 2004, **126**, 4486–4487.
114 L. Serre, A. Sailland, D. Sy, P. Boudec, A. Rolland, E. Pebay-Peyroula and C. Cohen-Addad, *Structure*, 1999, **7**, 977–988.
115 M. L. Neidig, O. W. Choroba, J. B. Spencer and E. I. Solomon, unpublished results.
116 R. A. Scott, S. K. Wang, M. K. Eidsness, A. Kriauciunas, C. A. Frolik and V. J. Chen, *Biochemistry*, 1992, **31**, 4596–4601.
117 C. R. Randall, Y. Zang, A. E. True, L. Que, J. M. Charnock, C. D. Garner, Y. Fujishima, C. J. Schofield and J. E. Baldwin, *Biochemistry*, 1993, **32**, 6664–6673.
118 R. W. Busby and C. A. Townsend, *Bioorg. Med. Chem.*, 1996, **4**, 1059–1064.
119 T. K. Wu, R. W. Busby, T. A. Houston, D. B. Mcilwaine, L. A. Egan and C. A. Townsend, *J. Bacteriol.*, 1995, **177**, 3714–3720.
120 S. W. Elson, K. H. Baggaley, M. Davison, M. Fulston, N. H. Nicholson, G. D. Risbridger and J. W. Tyler, *J. Chem. Soc., Chem. Commun.*, 1993, 1212–1214.
121 J. E. Baldwin, M. D. Lloyd, B. Whason, C. J. Schofield, S. W. Elson, K. H. Baggaley and N. H. Nicholson, *J. Chem. Soc., Chem. Commun.*, 1993, 500–502.
122 S. F. Yang and N. E. Hoffman, *Annu.Rev. Plant Physiol. Plant Molec. Biol.*, 1984, **35**, 155–189.
123 J. C. Fernandez-Maculet, J. G. Dong and S. F. Yand, *Biochem. Biophys. Res. Commun.*, 1993, **193**, 1168–1173.
124 J. Zhou, A. M. Rocklin, J. D. Lipscomb, L. Que and E. I. Solomon, *J. Am. Chem. Soc.*, 2002, **124**, 4602–4609.
125 A. M. Rocklin, D. L. Tierney, V. Kofman, N. M. W. Brunhuber, B. M. Hoffman, R. E. Christoffersen, N. O. Reich, J. D. Lipscomb and L. Que, Jr., *Proc. Natl. Acad. Sci. U. S. A.*, 1999, **96**, 7905–7909.
126 R. H. Holm, P. Kennepohl and E. I. Solomon, *Chem. Rev.*, 1996, **96**, 2239–2314.
127 H. J. Lee, M. D. Lloyd, K. Harlos, I. J. Clifton, J. E. Baldwin and C. J. Schofield, *J. Mol. Biol.*, 2001, **308**, 937–948.
128 K. S. Hewitson, L. A. McNeill, M. V. Riordan, Y. M. Tian, A. N. Bullock, R. W. Welford, J. M. Elkins, N. J. Oldham, S. Bhattacharya, J. M. Gleadle, P. J. Ratcliffe, C. W. Pugh and C. J. Schofield, *J. Biol. Chem.*, 2002, **277**, 26351–26355.
129 S. M. Hecht, *J. Nat. Prod.*, 2000, **63**, 158–168.
130 J. N. Kemsley, K. Loeb Zaleski, M. S. Chow, A. Decker, E. Y. Shishova, E. C. Wasinger, B. Hedman, K. O. Hodgson and E. I. Solomon, *J. Am. Chem. Soc.*, 2003, **125**, 10810–10821.
131 J. N. Kemsley, E. C. Wasinger, S. Datta, N. Mitic, T. Acharya, B. Hedman, J. P. Caradonna, K. O. Hodgson and E. I. Solomon, *J. Am. Chem. Soc.*, 2003, **125**, 5677–5686.
132 F. Neese and E. I. Solomon, *J. Am. Chem. Soc.*, 1998, **120**, 12829–12848.
133 C. Walling, M. Kurz and H. J. Schugar, *Inorg. Chem.*, 1970, **9**, 931–937.
134 R. M. Burger, *Struct. Bonding*, 2000, **97**, 287–303.
135 F. Neese, J. M. Zaleski, K. Loeb Zaleski and E. I. Solomon, *J. Am. Chem. Soc.*, 2000, **122**, 11703–11724.
136 E. I. Solomon, A. Decker and N. Lehnert, *Proc. Natl. Acad. Sci. U. S. A.*, 2003, **100**, 3589–3594.
137 N. Lehnert, F. Neese, R. Y. N. Ho, L. Que, Jr. and E. I. Solomon, *J. Am. Chem. Soc.*, 2002, **124**, 10810–10822.
138 L. Worth, B. L. Frank, D. F. Christner, M. J. Absalon, J. Stubbe and J. W. Kozarich, *Biochemistry*, 1993, **32**, 2601–2609.
139 G. V. Buxton, C. L. Greenstock, W. P. Helman and A. B. Ross, *J. Phys. Chem. Ref. Data*, 1988, **17**, 513–886.
140 D. T. Sawyer, C. Kang, A. Llobet and C. Redman, *J. Am. Chem. Soc.*, 1993, **115**, 5817–5818.
141 J. D. Tan, S. E. Hudson, S. J. Brown, M. M. Olmstead and P. K. Mascharak, *J. Am. Chem. Soc.*, 1992, **114**, 3841–3853.
142 W. Wu, D. E. Vanderwall, S. Teramoto, S. M. Lui, S. T. Hoehn, X. J. Tang, C. J. Turner, D. L. Boger, J. W. Kozarich and J. Stubbe, *J. Am. Chem. Soc.*, 1998, **120**, 2239–2250.
143 C. A. Grapperhaus, B. Mienert, E. Bill, T. Weyhermuller and K. Wieghardt, *Inorg. Chem.*, 2000, **39**, 5306–5317.
144 M. H. Lim, J. U. Rohde, A. Stubna, M. R. Bukowski, M. Costas, R. Y. N. Ho, E. Munck, W. Nam and L. Que, *Proc. Natl. Acad. Sci. U. S. A.*, 2003, **100**, 3665–3670.
145 J. U. Rohde, J. H. In, M. H. Lim, W. W. Brennessel, M. R. Bukowski, A. Stubna, E. Munck, W. Nam and L. Que, *Science*, 2003, **299**, 1037–1039.
146 W. Balland, M. F. Charlot, F. Banse, J. J. Girerd, T. A. Mattioli, E. Bill, J. F. Bartoli, P. Battioni and D. Mansuy, *Eur. J. Inorg. Chem.*, 2004, 301–308.
147 A. Decker, J. U. Rohde, L. Que and E. I. Solomon, *J. Am. Chem. Soc.*, 2004, **126**, 5378–5379.